4-1985

Resonant Electron Transfer and K-Shell Excitation of Lithiumlike Projectiles in Collisions with Neutral Gas Targets

Carollyn Sloan Oglesby
Western Michigan University

RESONANT ELECTRON TRANSFER AND K-SHELL EXCITATION OF LITHIUMLIKE PROJECTILES IN COLLISIONS WITH NEUTRAL GAS TARGETS

by

Carollyn Sloan Oglesby

A Thesis
Submitted to The
Faculty of the Graduate College
in partial fulfillment of the
requirements for the
Degree of Master of Arts
Department of Physics

Western Michigan University
Kalamazoo, Michigan
April 1985

ACKNOWLEDGEMENTS

The execution and completion of this work was made not only possible, but thoroughly enjoyable through association with my research advisors, Dr. John Tanis and Dr. Eugene Bernstein. I wish to thank them for allowing me many professional opportunities and experiences in representing my own research not ordinarily granted to a Master's degree candidate. Whatever contribution I may have made to the study of Resonant-Transfer- and Excitation was made possible through their assistance and by the trust and confidence which they placed in me.

I am indebted to Mark Clark, Bill Graham and David Hughes for their contributions to the technical aspects of this project. I would like to thank Dr. Michi Soga for the part he played as one of my thesis committee members and also for his patient and inspirational teaching of physics. Jaleh Owliaei's patience in previewing my presentations and her unconditional support and friendship were invaluable in the course of this work.

This work would not have been accomplished without the continual support of my husband, Tom, given freely in spite of the demands of his own professional career. My children, Lauren and Doug, have given me renewed strength time and again through their love and all of the pleasant diversions of childhood. I also wish to thank my mother, for her love and great expectations.

My thanks is extended to the Graduate College of WMU for the financial assistance granted for my travel to Brookhaven. The support of this research by the United States Department of Energy is gratefully acknowledged.

Carollyn Sloan Oglesby

Oglesby, Carollyn Sloan

RESONANT ELECTRON TRANSFER AND K-SHELL EXCITATION OF LITHIUMLIKE PROJECTILES IN COLLISIONS WITH NEUTRAL GAS TARGETS

Western Michigan University M.A. 1985

TABLE OF CONTENTS

LIST OF TABLES

LIST OF FIGURES

CHAPTER I

INTRODUCTION

The events which can occur when a projectile ion collides with a neutral target atom can be divided into three major catagories: excitation, ionization, and charge transfer (Hasted, 1972). These processes can occur in either collision partner or in both, and combinations of these processes can occur as well. In a broad sense, the three processes are related since they can be attributed to the Coulomb force between the interacting particles, and occur commonly in the direct interaction between the nucleus of one colliding partner and the electrons of the other. They are dependent upon the distance between the particles, the charge state, and the energy at which the collision takes place. These processes can be described schematically by considering transitions between atomic energy levels.

In excitation, one or more electrons are excited from lower to higher energy states within the atom or ion. The result of a single electron excitation is the production of a vacancy in the energy level originally occupied by the excited electron. Ionization is characterized by the loss of one or more electrons. If a target atom is ionized and the lost electron is captured by the projectile, then the process is referred to as charge transfer.

The occurrence of any of these events is verifiable upon detection of energy or particles emitted in the decay of the excited species or by detection of a charge-changed projectile or target. The decay of the

excited state can proceed in one of two ways: by photon emission, in which case the number of electrons in the projectile is left unchanged, or by autoionization, i.e., the Auger process (Merzbacher, 1970), in which one electron fills the vacancy and is accompanied by simultaneous ejection of another electron (termed an Auger electron). In this case, the total positive charge on the projectile is increased by one. The Auger process will be discussed in detail later.

It was mentioned that combinations of excitation, ionization, and charge transfer occur in the projectile ion and/or the target atom in an ion-atom collision. The example which is of interest in this thesis is the combination of electron capture and excitation of the projectile ion in a single collision. In principle, any excitation is possible, but only those which give rise to K-shell vacancies will be considered here, so discussion is limited to those excitations in which an electron is promoted from $n=1$ to $n\geq 2$. The electron which is captured may enter any unoccupied bound state of the ion. Immediately after the collision there may exist a vacancy in the $n=1$ state or K-shell, of an ion which has gained an electron. This charge-changed excited state will decay by emitting either a photon or an electron. Those events which result in single capture and K-shell excitation (and thus yield an intermediate excited state) followed by x-ray emission, are the primary emphasis of this thesis.

In collisions between highly charged projectiles and neutral gas targets, there are two mechanisms by which this combined electron transfer and ion excitation can proceed. One is a two-step process called Non-Resonant-Transfer-and-Excitation, or NTE (Pepmiller, 1983),

in which the projectile is first excited through the Coulomb interaction with the target nucleus and subsequently captures an electron from the target. Deexcitation by x-ray emission follows. In the formation of the excited state, the excitation and capture events are uncorrelated. In the other mechanism of formation of the intermediate excited state, both transfer and excitation take place simultaneously, and again, de-excitation occurs by x-ray emission. This process is called Resonant-Transfer-and-Excitation, or RTE (Tanis et al., 1981 and Tanis et al., 1982).

A mechanism analogous to RTE, called Dielectronic Recombination, or DR (Seaton and Storey, 1976), which can yield the same intermediate excited state, occurs in the interaction between an ion and a free electron. It is believed that the RTE process bears a close resemblence to DR and hence the theory of RTE to be discussed requires some preliminary understanding of DR. DR has been implicated as a mechanism of energy dissipation in fusion plasmas (Post, 1981; Burgess, 1964 and 1965; Bitter et al., 1979; and Merts, Cowan and Magee, 1976), where free electrons abound. The energy is carried away from the plasma confinement area by the photon which is given off in the relaxation of the excited state. The effort which is being applied to make fusion feasible for energy production has made DR a topic of active experimental investigation over the last two decades. Since fusion also occurs in interstellar processes, DR is of interest in astrophysical research endeavors as well (Burgess, 1964). Laboratory measurements of DR are difficult to obtain -- in general, the methods utilize crossed or merged beams of ions and electrons (Belic, Dunn, Morgan, Mueller and Timmer, 1983; Dittner

et al., 1983; and Mitchell et al., 1982).

RTE then, is of interest not only in its own right as a fundamental atomic process, but also because of its similarity to DR. The RTE process was proposed in 1980 (Tanis et al., 1982), and the evidence in support of its close relationship to DR has not yet been proven conclusively. Reports of several recent experiments (Tanis et al., 1982; Tanis et al., 1984 and Tanis et al., in press) make the connection plausible, however, since the results of the experiments so far have quantitatively and qualitatively reflected the outcome which is predicted (Oglesby, Bernstein and Tanis, 1984) by a theory of RTE (Brandt, 1983a) which rests upon its purported similarity to DR. If the relationship between DR and RTE is proven, study of RTE could well provide a means of studying DR, since in contrast to DR experiments, RTE experiments are relatively easy to perform.

It is the purpose of this thesis to present a portion of the evidence which supports the hypothesis of the process of RTE and the relationship between RTE and DR. Chapter II contains a qualitative discussion of processes pertinent to an understanding of RTE. In Chapter III, the theory of RTE will be outlined in such a way as to emphasize its similarity to DR. Calculations of RTE cross sections predicted by the theory and trends which arise when the projectiles and targets are independently varied will be examined. In Chapter IV, an RTE experiment in which the author was a participant, will be discussed and the method of calculation of all experimental cross sections of interest will be explained. The results will be examined in Chapter V, which also contains the comparison of theoretical calculations to the results

of the experiment discussed in Chapter IV and two similar experiments. Chapter VI summarizes the conclusions resulting from this work. Two appendices follow. The first contains the program which performed the theoretical calculations and the second outlines the calculation of all pertinent experimental cross sections.

CHAPTER II

RELATED PROCESSES

The Auger Process

Both RTE and DR take place via the time-reversed Auger process. Time reversal assumes that the system passes through exactly the same states as in the forward process but in the reverse order. So that the analogy between RTE (and DR) and the Auger process may be made clear, examination of the Auger process follows.

Assume the existence of an excited state in an atom or ion which contains at least two electrons. The vacancy must occur in a shell which is lower in energy than both of the electrons which will take part in the process. The simplest case would be a doubly excited helium atom with two K-shell vacancies; however, for ease of comparison to the system which will be used to examine RTE in this work, we start with a system of four electrons (Fig. 1). The orbital angular momentum of the excited state has been left unspecified. Further discussion of the possible excited states will follow, and for now it is sufficient to note that there are many possible excited electron configurations which will deexcite by the Auger mechanism.

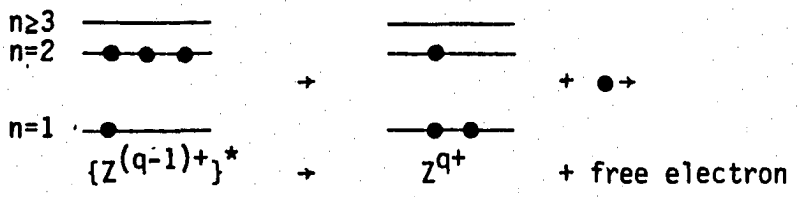

Figure 1. Schematic of the Auger process for a four electron ion with a vacancy in the K-shell.

The decay of such an excited state will proceed either by photon emission or by electron emission. Photon emission is part of the RTE and DR processes and so discussion of this decay mode is made in the sections pertaining to these processes. Figure 1 depicts electron emission (or the Auger process), which occurs in the system when one electron falls to the K-shell without emission of radiation. Simultaneously, the energy supplied by this transition is transferred to another electron, which is ejected. The ejected electron is referred to as an Auger electron. Energy is conserved in the process so that the kinetic energy, ε_r, of the Auger electron depends upon the energy difference between the excited and ground states of the relaxing ion, E_{trans}, and upon the binding energy of the ejected electron, E_b, before its departure:

$$\varepsilon_r = E_{trans} - E_b . \qquad (2.1)$$

Since the energies of the electrons in the initial and final states of the relaxing ion have discrete values, the energy carried away by the Auger electron is a well-defined quantity for any particular Auger transition.

Since the decay of the excited state is limited to either Auger electron emission or photon emission, the Auger electron yield is given by

$$Y = 1 - \omega . \qquad (2.2)$$

Here ω is the fluorescence yield which includes all transitions which

give rise to photons. Which of the decay modes will predominate depends upon the intermediate state of the ion and its atomic number (Hasted).

In summary, it is of importance to note that in the Auger process, deexcitation and electron emission are simultaneous. Auger emission is a resonant process which occurs only if, but not necessarily when, $E_{trans} \geq E_b$, and results in a quantization of the kinetic energy of the Auger electron.

Dielectronic Recombination

The process of Dielectronic Recombination (DR) involves the radiationless capture of a free electron into a bound state of an ion along with the simultaneous excitation of the ion. The relative kinetic energy between the ion and the captured electron supplies the energy required for excitation. The process of DR is completed after the excited state decays by photon emission (Fig. 2).

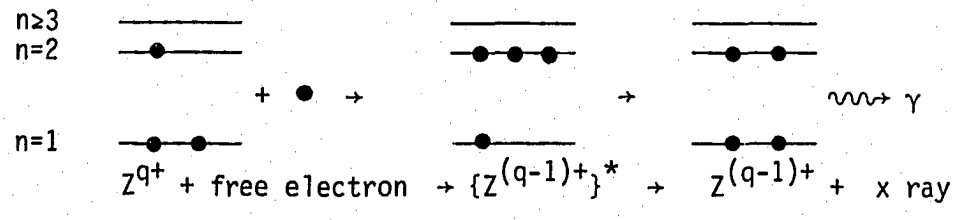

Figure 2. Schematic of Dielectronic Recombination. Simultaneous ion excitation and capture of free electron followed by photon emission.

Reversing the Auger process shown in Figure 1 and comparing it to the first two steps of Figure 2 shows that the formation of the excited state of DR is qualitatively identical to the time-reversed

Auger transition. Since time reversal only affects the order of events, and since the Auger transition is a resonant process, DR must also be a resonant process. Like the Auger transition, DR depends upon the energy difference between the initial and final (resonance) states of the projectile ion. In the rest frame of the ion, the energy of the incoming electron must equal the corresponding Auger energy for the transition which will take place. In terms of the velocities, the resonance condition occurs when the relative velocity of the projectile ion and the electron matches the velocity of the Auger electron.

Ideally, a direct measurement of DR would be obtained by accelerating the projectile beam through a static target of free electrons; however, such a target is not easily constructed. The DR experiments which have been successful have employed crossed (Belic et al., 1983) and merged (Dittner et al., 1983 and Mitchell et al., 1983) beams of ions and electrons. Very high vacuums are required, since free electrons by nature are prone to capture with a high probability by surrounding atoms or molecules. Therefore even a low backgroud gas density can give relatively large errors. Other errors and uncertainties result from low particle density in the beam and inhomogeneity of the beams, so that assumptions must be made regarding the number of particles which are actually contained within the interaction region. Because of the low beam density, long running times are generally required to collect a significant number of events.

Several theoretical calculations of DR cross sections have been performed (Roszmann, 1979; LaGattuta and Hahn, 1983; McLaughlin and

Hahn, 1982; Nasser and Hahn, 1983, and Hahn in a private communication, October 3, 1983). In some cases the experimental results differ appreciably from the calculated results. McLaughlin and Hahn (1982), Nasser and Hahn (1983) and Hahn (personal communication, October 3, 1983) have reported calculated DR cross sections for the systems to be examined and it is these data which are used in the calculation of RTE. A few important features of these data will be discussed. Additional pertinent points will be taken up in further detail in the section on RTE calculations. The cross sections for DR in lithiumlike sulfur are shown as functions of Auger energy in Figure 4 and Table 1. Each peak represents the probability that a particular excited state will be formed in the simultaneous capture and excitation event. The notation, {n,n}, indicates which of the intermediate excited states is represented by each peak, where the indices represent the principal quantum numbers of the orbitals into which the capture and excitation events occur. The notation is unambiguous, since once the excited state has been formed, the captured and excited electrons are indistinguishable. The first two DR peaks, {2,2}, can decay by emitting only a K_α x ray, which is defined as the x ray resulting from the transition of an electron from n=2 to n=1 (Fig. 3). All other transitions, n>2 to n=1, are denoted as K_β x rays. The remainder of the DR peaks, {2,≥3}, can give

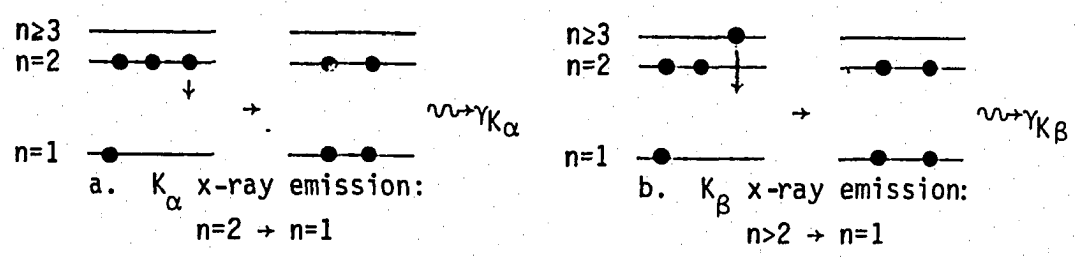

Figure 3. K_α and K_β x-ray emission

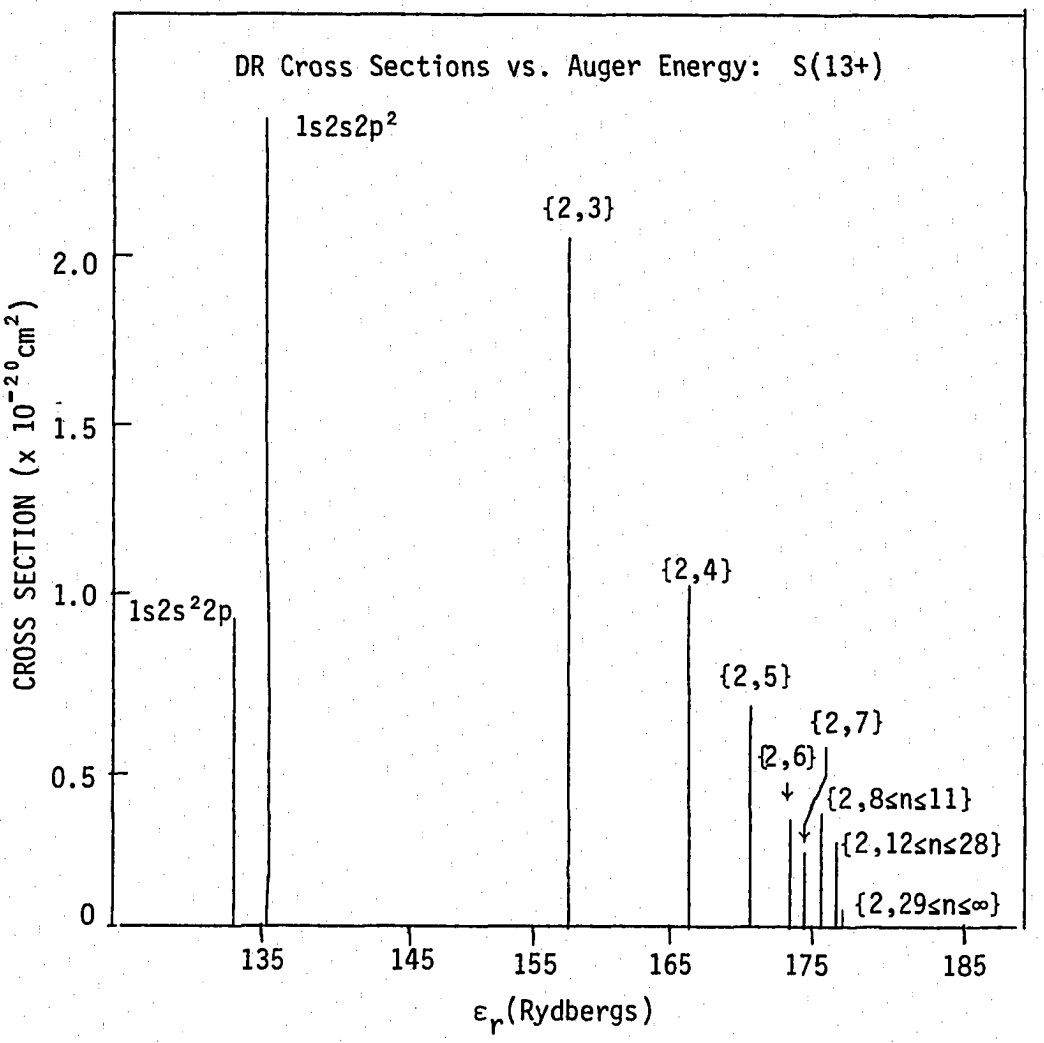

Figure 4. Calculated Dielectronic Recombination cross sections for lithiumlike sulfur, S(13+). Numbers in brackets indicate principal quantum states of electrons participating in formation of resonance state.

Table 1

Calaulated DR data for S(13+) from McLaughlin and Hahn (1982).

excited state {n,n}	electron configuration	ϵ_r(Rydbergs)	σ_{DR}($\times 10^{-20}$ cm^2)
{2,2}	$1s2s^22p$	133.6	0.897
{2,2}	$1s2s2p^2$	136.0	2.396
{2,3}	$1s2s^23p$	157.3	0.088
	1s2s2p3s	157.7	0.250
	1s2s2p3p	158.3	1.035
	1s2s2p3d	159.0	0.540
{2,4}	$1s2s^24p$	166.2	0.016
	1s2s2p4s	166.9	0.122
	1s2s2p4p	167.2	0.588
	1s2s2p4d	167.5	0.277
	1s2s2p4f	167.6	0.017
{2,5}	$1s2s^25p$	170.3	0.005
	1s2s2p5s	171.0	0.050
	1s2s2p5p	171.2	0.350
	1s2s2p5l (l=2,3)	171.4	0.162
{2,6}	1s2s2p6l (l=0,1)	173.4	0.250
	1s2s2p6l (l=2,3)	173.5	0.097
{2,7}	1s2s2p7l ($0 \geq l \geq 3$)	174.7	0.225
{2,8$\geq$n$\geq$11}	1s2s2pnl ($0 \geq l \geq 3$)	176.5	0.379
{2,12$\geq$n$\geq$28}	1s2s2pnl ($0 \geq l \geq 3$)	177.5	0.237
{2,29$\geq$n$\geq\infty$}	1s2s2pnl ($0 \geq l \geq 3$)	178.0	0.041

rise to either a K_α or a K_β x ray, since there is always an n=2 electron present.

These calculations included individual orbital angular momentum states in the projectile, as shown more clearly in Table 1. The S(13+) data are those which are shown in Figure 4. Note that only states are listed in which either the captured or the excited electron goes to the L-shell, i.e., all states are of the form {2,≥2}. There is some probability that the states {≥3,≥3} could be formed in DR. The decay of such states could yield K_α or K_β x rays. DR cross section data for these states are not available, however.

It is important to note that the series of events which occurs in DR is identical to that which takes place in RTE. The sole distinction between the two processes is in the source of electrons for capture; in DR the electrons are initially free while in RTE they are initially bound in a neutral atom. The excited intermediate states and their subsequent decay by photon emission are qualitatively indistinguishable. The resonance condition - that the relative velocity of the electron and the ion match the velocity of the corresponding Auger electron - is exactly the same for RTE as it is for DR. Further discussion of RTE and its relationship to DR is the subject of Chapter III.

Non-Resonant-Transfer-and-Excitation

Non-Resonant-Transfer-and-Excitation (NTE) is believed to be a two-step process which can give rise to the same intermediate excited states as RTE and DR. Though the mechanism of NTE is unrelated to the mechanism of RTE (and DR), the resulting excited intermediate states

and their subsequent decay by photon emission are experimentally indistinguishable from those of RTE. NTE must therefore be considered as a competing process. A recently proposed theory of NTE suggests that the magnitude of the NTE cross section at the RTE resonance energy is small for the system under study (Brandt, 1983b).

In NTE, the formation of the intermediate excited state occurs by excitation of a projectile electron through the Coulomb interaction with the target nucleus (Fig. 5). In the same encounter, an electron is transferred from the target to the projectile. The capture and excitation events are uncorrelated. In the energy range considered

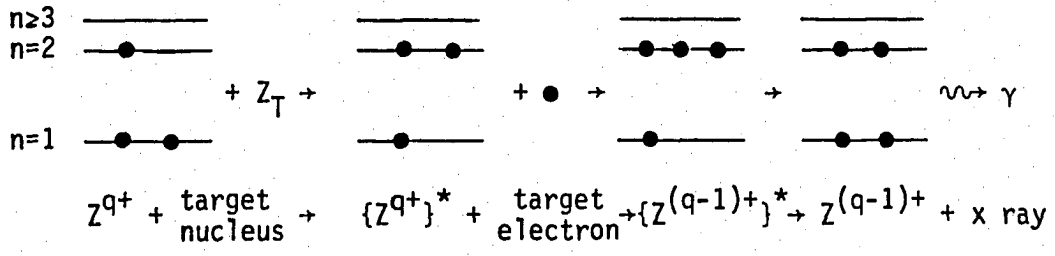

Figure 5. Non-Resonant-Transfer-and-Excitation. Coulomb excitation of projectile with subsequent electron capture followed by photon emission.

for NTE, excitation is regarded as the rate-limiting step of the process since the cross section for excitation is roughly two orders of magnitude smaller than the cross section for capture. The general shapes of the capture and excitation cross sections for highly charged projectile ions incident on neutral target atoms are given in Figure 6. The cross section for the capture process is large at low energy and decreases exponentially as the energy is increased. The excitation cross section rises fairly rapidly at low energy, reaches a maximum and then slowly decreases (Sellin, 1979 and Hasted, 1972).

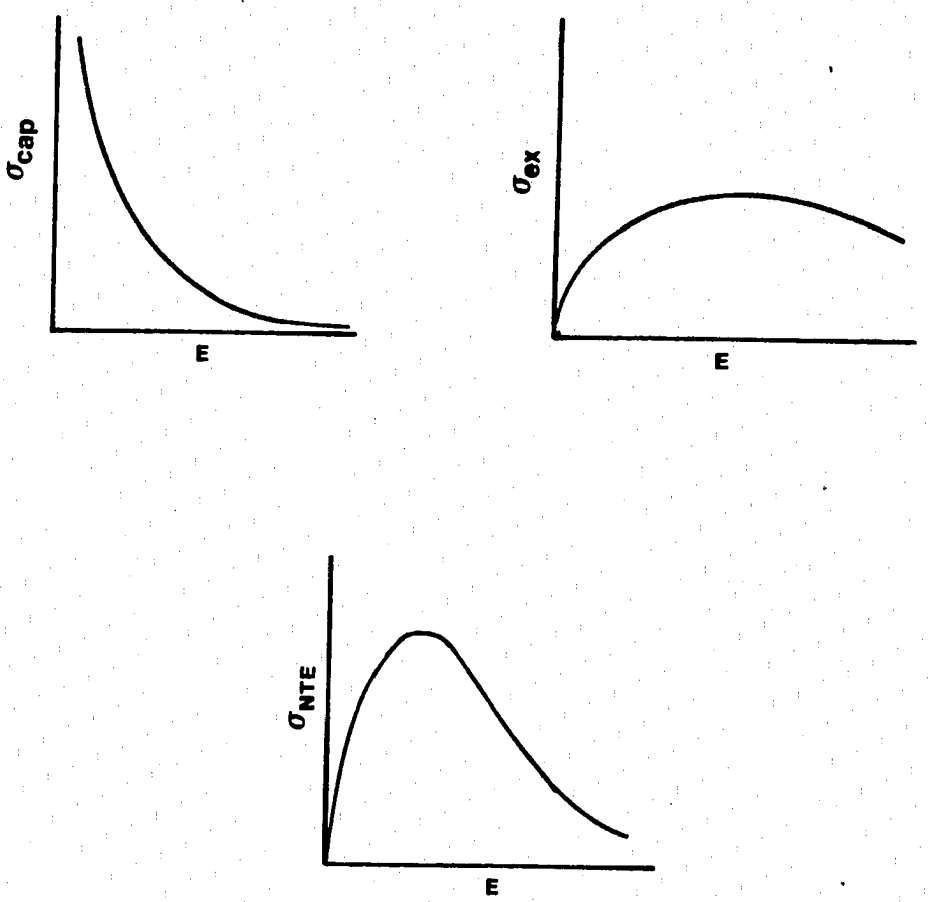

Figure 6. Qualitative shapes of capture, excitation, and NTE cross sections. The shape of the NTE cross section curve is given by the product of the capture and excitation cross section curves.

The probabilities for both capture and excitation are dependent upon b, the impact parameter. Since for NTE both processes must occur, the cross section for NTE, σ_{NTE}, is proportional to the product of the probabilties, P(b), of capture and excitation (Pepmiller, 1983).

$$\sigma_{NTE} = 2\pi \cdot \int_0^\infty P_{cap}(b) \cdot P_{ex}(b) \cdot bdb. \qquad (2.3)$$

The integral is over all impact parameters. Over the range of nonzero P_{ex}, the probability for capture is approximately constant and equal to P_{cap} at zero impact parameter, and so $P_{cap}(0)$ can be taken out of the integral,

$$\sigma_{NTE} \simeq P_{cap}(0)\{2\pi \cdot \int_0^\infty P_{ex}(b) \cdot bdb\} \qquad (2.4)$$

or

$$\sigma_{NTE} \simeq P_{cap} \cdot \sigma_{ex} \qquad (2.5)$$

since the quantity in brackets in equation (2.4) is just the excitation cross section. The behavior of the cross section for NTE is calculated to have a maximum at low energy (approximately 25 MeV for S(13+) + He) and to exponentially decrease with increasing projectile energy. Qualitatively this is the shape obtained by multiplying σ_{ex} into σ_{cap} (Fig. 6).

The projectile energy dependence and magnitude of the NTE peak will vary depending upon the charge state of the projectile and its atomic number, Z_P, and upon the atomic number of the target, Z_T. With higher Z_T, the Coulomb attraction between the target nucleus and the projectile electrons becomes stronger, increasing the probability for projectile excitation. Also, since the number of electrons in the

target is increased, the capture probability is increased. To investigate RTE then, it is expected that a low Z target is preferable in order to minimize the NTE contribution.

Figure 7 shows the calculated NTE cross section for S(13+) incident on He (Brandt, 1983b). The resonant peak for RTE is expected to occur at about 130 MeV, far above the energy where σ_{NTE} has its predicted maximum. A rigorous quantum mechanical treatment of RTE and NTE has been developed by Feagin, Briggs and Reeves (1984), but will not be considered in this work. Suffice it to say that the results of Feagin's treatment are consistent with the results of the theory of Brandt (1983a) which will be discussed in Chapter III.

Experiments designed to investigate NTE are essentially the same as those designed to investigate RTE (Chapter IV, Section 1) but require lower projectile energy. To date, only three NTE experiments have been reported (Pepmiller, 1983; Clark, Brandt and Shafroth, 1984 and Tanis et al., in press). Only Tanis, et al.(in press) have utilized the projectile/target system which is of interest in this work. Further experimental work is needed to more fully understand NTE and its relevance to RTE studies.

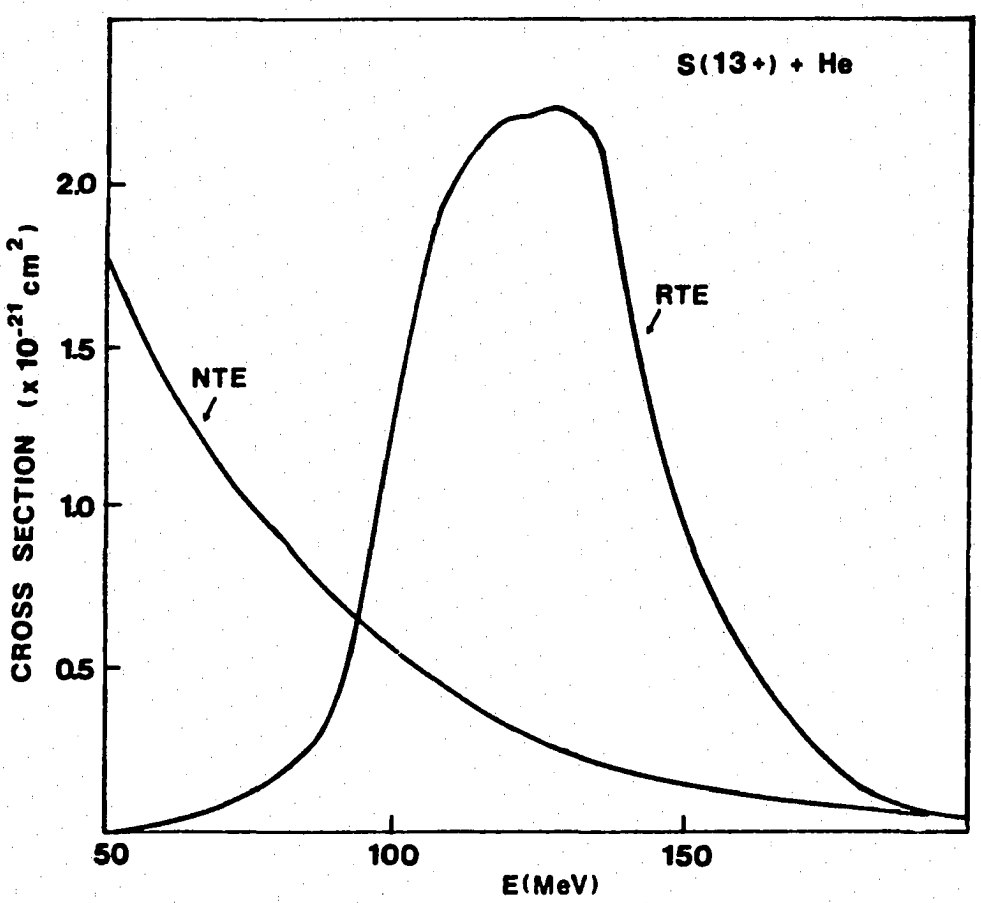

Figure 7. Calculated energy dependence of RTE and NTE cross sections for S(13+) incident on He.

CHAPTER III

RESONANT-TRANSFER-AND-EXCITATION: THEORY

The Process

As was noted in Chpater II, RTE is very similar to DR. RTE occurs in an ion-atom collision when simultaneous excitation of the ion and capture of a target electron are followed by electron relaxation which results in an x ray. The excitation and capture occur only when the relative velocity of the projectile ion and the incoming electron matches the velocity of the ejected Auger electron (in the inverse process) for the resonance state formed. All events of interest in this work occur in the projectile. No consideration is given to the fate of the target after it gives up an electron. A schematic representation of RTE is given in Figure 8. The similarity to Figure 2, representing the DR process, is evident.

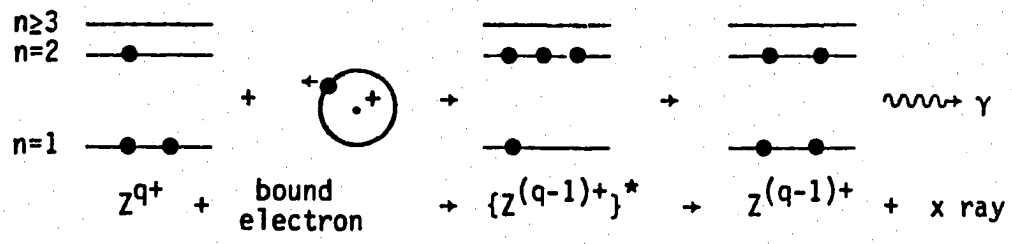

Figure 8. Resonant-Transfer-and-Excitation. Simultaneous ion excitation and capture of bound target electron followed by photon emission.

Theory

The theory of RTE as presented by Brandt (1983a) is derived from the

impulse approximation, which essentially states that immediatedly after the collision, the separation between the projectile and target is such that there can be no further interaction. This requires that $v_{ion} >> v_{electron}$. The RTE energies for the systems considered here (i.e. at K-shell excitation energies) satisfy this assumption for the outer shell, weakly bound electrons. The result of the theory, and the equation upon which all theoretical calculations are based, is (Brandt, 1983a):

$$\sigma_{RTE}^{\{n,n\}} = \{M/2E\}^{\frac{1}{2}} \cdot \sigma_{DR} \cdot \sum_i J_i(p_{iz}), \qquad (3.1)$$

where $\sigma_{RTE}^{\{n,n\}}$ is the RTE cross section for the formation of the resonance state {n,n}, M and E are the mass and energy of the projectile ion respectively, σ_{DR} is the DR cross section, and $J_i(p_{iz})$ is the Compton profile (momentum distribution) of the target. The DR cross sections were discussed in Chapter II. The Compton profile term results from the fact that the electrons available for capture are now bound to the nucleus of a target atom. The electrons bound in any given target atom have a distribution of momenta (and therefore velocities) depending upon the quantum numbers n and l of the occupied bound state. This momentum distribution is known as the Compton profile, and has been calculated using Hartree Fock and relativistic Dirac Hartree Fock wave functions for atoms with $1 \geq Z \geq 102$ by Biggs, Mendelsohn and Mann (1975).

The Compton profile for the electrons in a neutral, ground state atom is a symmetric Gaussian function of momentum, p, centered about

p=0. The notation, p_{iz}, in $J_i(p_{iz})$ represents the z component of momentum (the component along the beam axis) of the i^{th} electron in the target. Electrons with the same $\Psi_{n,l}$ wave function have the same probability of having a particular value of momentum in any particular direction. Graphical representations of the Compton profiles for He and Ar are given in Figures 9a and b. The relative width of the distribution increases with the number of electrons in the target. In equation (3.1), the Compton profile is summed over all electrons which can contribute to the formation of the resonance state {n,n}, i.e., those electrons available for capture which satisfy the impulse approximation (where $v_{ion} >> v_{electron}$), and can therefore contribute to RTE.

The Compton profile for the electrons in any given target is a continuous function of momentum. Hence, for relative velocities between the projectile and target electron which satisfy the resonance condition, there is a nonzero probability that an intermediate resonance state of RTE will be formed. Since these states are identical to the resonance states of DR, the Compton profile term in equation (3.1) effectively serves to broaden the sharply defined DR peak which corresponds to the particular resonance state formed. The extent to which the peak is broadened is proportional to the width of the Compton profile.

In the lab frame, the electron momentum of the target atom is negligible in comparison to the projectile momentum. In the rest frame of the ion, the momentum of the ith target electron along the beam axis as a

(a)

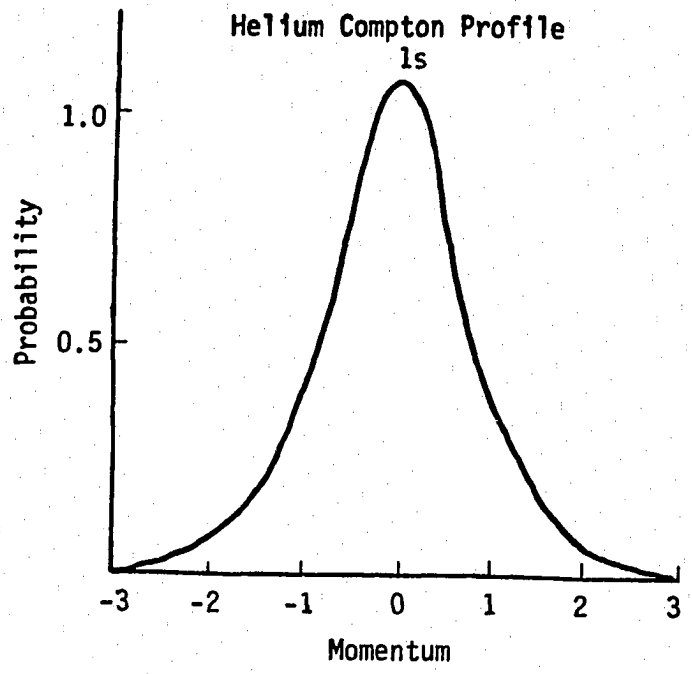

(b)

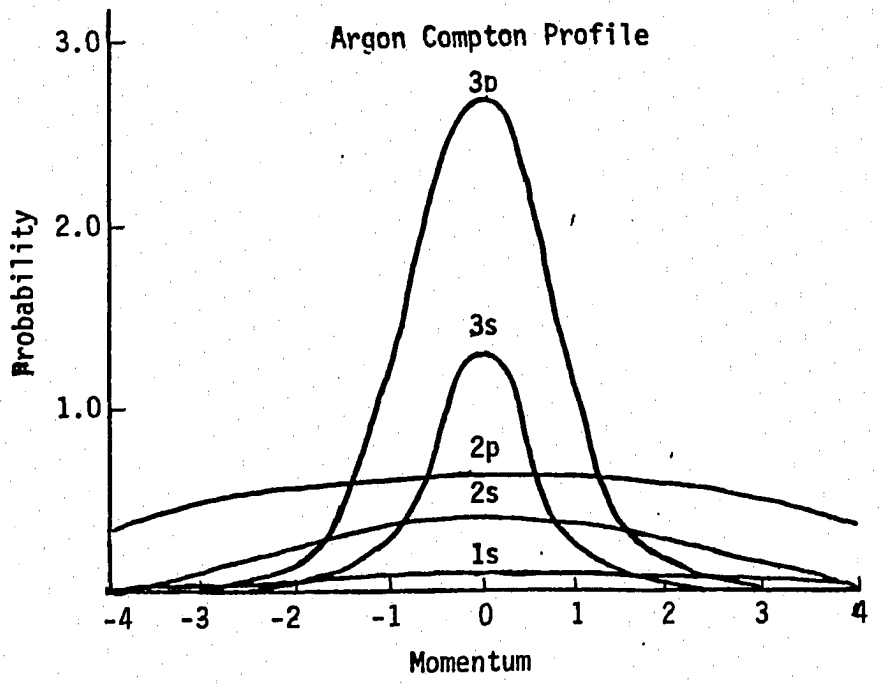

Figure 9. Compton profiles for (a) Helium and (b) Argon (from Biggs, Mendelsohn and Mann, 1975).

function of projectile energy, E, is given by

$$p_{iz} = (\varepsilon_r - Em/M)\cdot(M/2E)^{\frac{1}{2}}. \qquad (3.2)$$

where m is the mass of an electron. Since the Compton profile has its maximum at p_z equal to zero, the position of each broadened peak is transformed from the Auger energy to the laboratory frame projectile energy accordingly when equation (3.2) equals zero, that is, when

$$E = (\varepsilon_r M)/m. \qquad (3.3)$$

The overall effect of equation (3.1) can be summarized as follows: a peak in the projectile DR spectrum is broadened by having the target Compton profile superimposed upon it, and then transformed to the projectile lab frame energy. This is done for each of the DR peaks representing the {n,n} excited intermediate states. The contributions due to each peak are added together to obtain the total RTE cross section.

The above discussion indicates that the overall profile of the RTE cross section curve is dependent upon the positions and relative magnitudes of the DR cross sections of the projectile and upon the Compton profile of the target. The width of the Compton profile varies with the number and velocity of the target electrons, and therefore with the atomic number of the target, Z_T. The variation in magnitude of the individual DR peaks does not depend strongly on the atomic number of the projectile, Z_p. The intermediate resonance state energies for DR scale approximately with Z_p as

$$\varepsilon_{r_2} \simeq \varepsilon_{r_1}\cdot\{Z_{p_2}/Z_{p_1}\}^2. \qquad (3.4)$$

The numerical subscripts represent two distinct projectile species.

In scaling the DR transition energies from smaller to larger Z_p, the whole DR spectrum is shifted to higher energy and the energy separation between each resonance state increases.

Having considered the effect of the target Compton profile and the dependence of the resonance state energies of the projectile species on RTE, it is now possible to distinguish between two extreme cases of RTE profiles produced for different projectile/target systems. If the Compton profile is broad relative to the energy spacing between individual resonance states in the DR spectrum, the resulting RTE curve contains only one maximum (Fig. 10a). The individual resonance states, or groups of resonance states, cannot be resolved. This case corresponds to projectiles incident on a "heavy" target. On the other hand, if the Compton profile is narrow relative to the energy spacing between some of the individual resonance states or groups of resonance states in the DR spectrum, partial resolution of groups of resonance states is expected (Fig. 10b). This corresponds to a "heavy" projectile incident upon a "light" target.[†] In particular, the RTE spectrum is predicted to contain two maxima, the first representing the resonance states {2,2} and the remainder representing the resonance states $\{2,\geq 3\}$.

The resolution of these two groups of resonance states becomes significant when their decay by x-ray emission is reexamined. In Chapter II, it was stated that the {2,2} states can give rise only to K_α x rays ($n=2\rightarrow n=1$ transitions) while the group, $\{2,\geq 3\}$ give rise to both K_α and

[†]The relative terms "heavy" and "light" in this discussion are defined by the ratio of Z_p to Z_T in the projectile/target system under study. If $Z_p:Z_T$ is approximately equal to or greater than 10, then the projectile is "heavy" and the target is "light", and structure in the RTE profile may be observed.

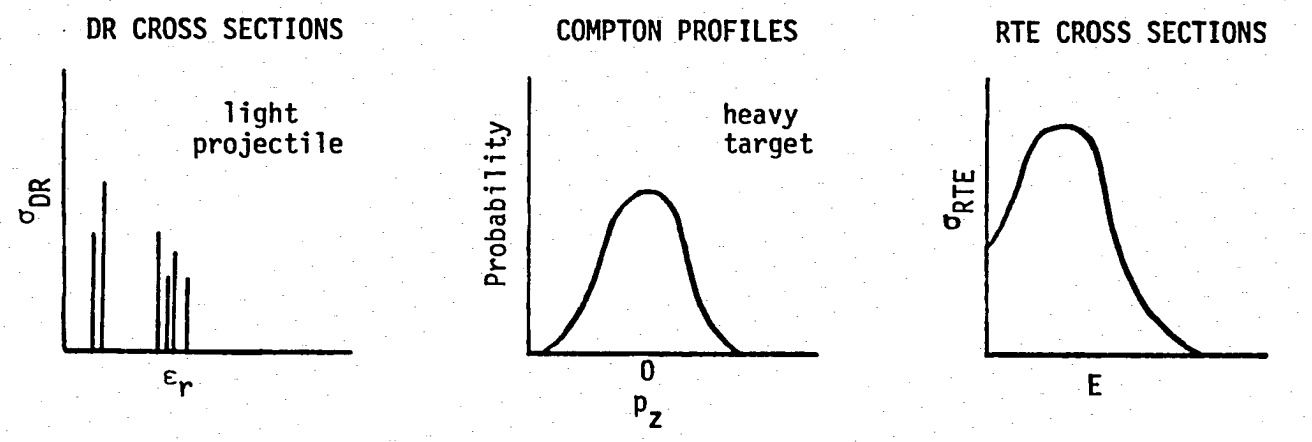

Figure 10. Predicted shapes of RTE cross section curves upon variation of projectile and target atomic weights.

K_β x rays ($n \geq 3 \rightarrow n=1$ transitions). Experimentally it is possible to distinguish between K_α and K_β x rays. Therefore, in addition to observing the correspondence between experimental and theoretical peak positions, it is also possible to verify the structure in the RTE cross section curve for the case of a heavy projectile and a light target.

As a final note, in the theory of Brandt (1983a), the initial binding energy of the target electrons has been neglected. Though this is believed to have a small effect on the overall cross section, its exclusion may contribute to the discrepancies between theory and experiment to be discussed in Chapter V.

Calculations

The program designed to perform the RTE calculations based on the theory of Brandt (1983a) is called OPUS3 and appears in Appendix A along with documentation. It was written in FORTRAN for the Dec-10 computer system currently in use at Western Michigan University. A brief description of its operation and capabilities follows, along with the results of sample calculations.

For each DR transition, calculation of p_{iz} is performed according to equation (3.2). After a linear interpolation of the published values of p_{iz} (Biggs, Mendelsohn and Mann, 1975) to match the calculated value, summation of the interpolated Compton profile over all contributing electrons is carried out. The individual RTE cross section for each DR transition, $\sigma_{RTE}^{\{n,n\}}$, is then calculated according to equation (3.1). Finally, all of the $\sigma_{RTE}^{\{n,n\}}$ values are added to yield the total

RTE cross section, σ_{RTE}, for a given beam energy.

The choice of target is limited in OPUS3 to H, He, Ne, Ar, or Xe, though only minor revisions would be required to add others. Scaling of projectile Auger energies from the S(13+) data of Hahn (personal communication, October 3, 1983) is automatic (eqn. 3.4) after the projectile Z_p is supplied. There is an option for limited linear scaling of the DR cross sections, which allows for user manipulation of the projectile data file to accomodate more refined cross section data as they become available. If no scaling of DR cross sections is performed, the S(13+) data are automatically used. Unscaled cross section calculations have been used to examine trends arising from the variation of colliding partners, as discussed in Section 2 of this chapter.

Figures 11a and b exemplify that discussion. Figure 11a shows the RTE calculation of projectiles with $14 \geq Z \geq 26$ incident on Ne, which, containing 10 electrons, is an example of a relatively heavy target. No structure in the RTE cross section is evident in the range of projectile Z studied. Figure 11b represents the same series of projectiles, but this time the target is He, which contains only two electrons, and therefore has a narrow momentum distribution. Structure becomes visible around Z_p = 18 (Ar) and is clearly evident in all heavier projectiles. Figure 12 shows more clearly the relationship between the separate DR peaks and the resulting structure in the RTE cross section for V(20+) on He. Note that the first peak corresponds to the {2,2} resonance states while the second peak corresponds to all the remaining states, i.e., {2,≥3}. In Figure 13, the {2,2} contribution to the

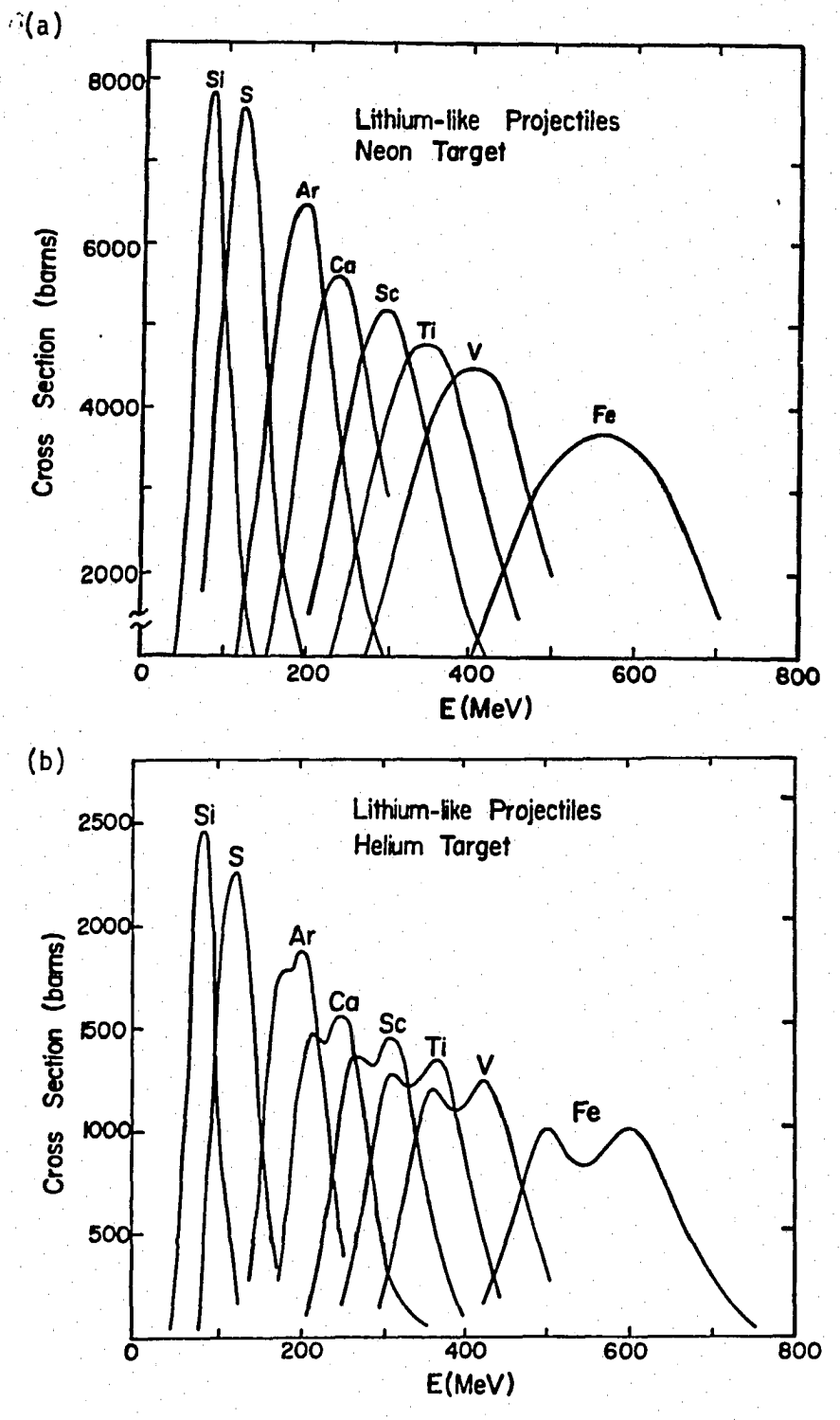

Figure 11. Calculated RTE cross sections for projectiles with $14 \leq Z \leq 26$ incident on (a) Neon and (b) Helium.

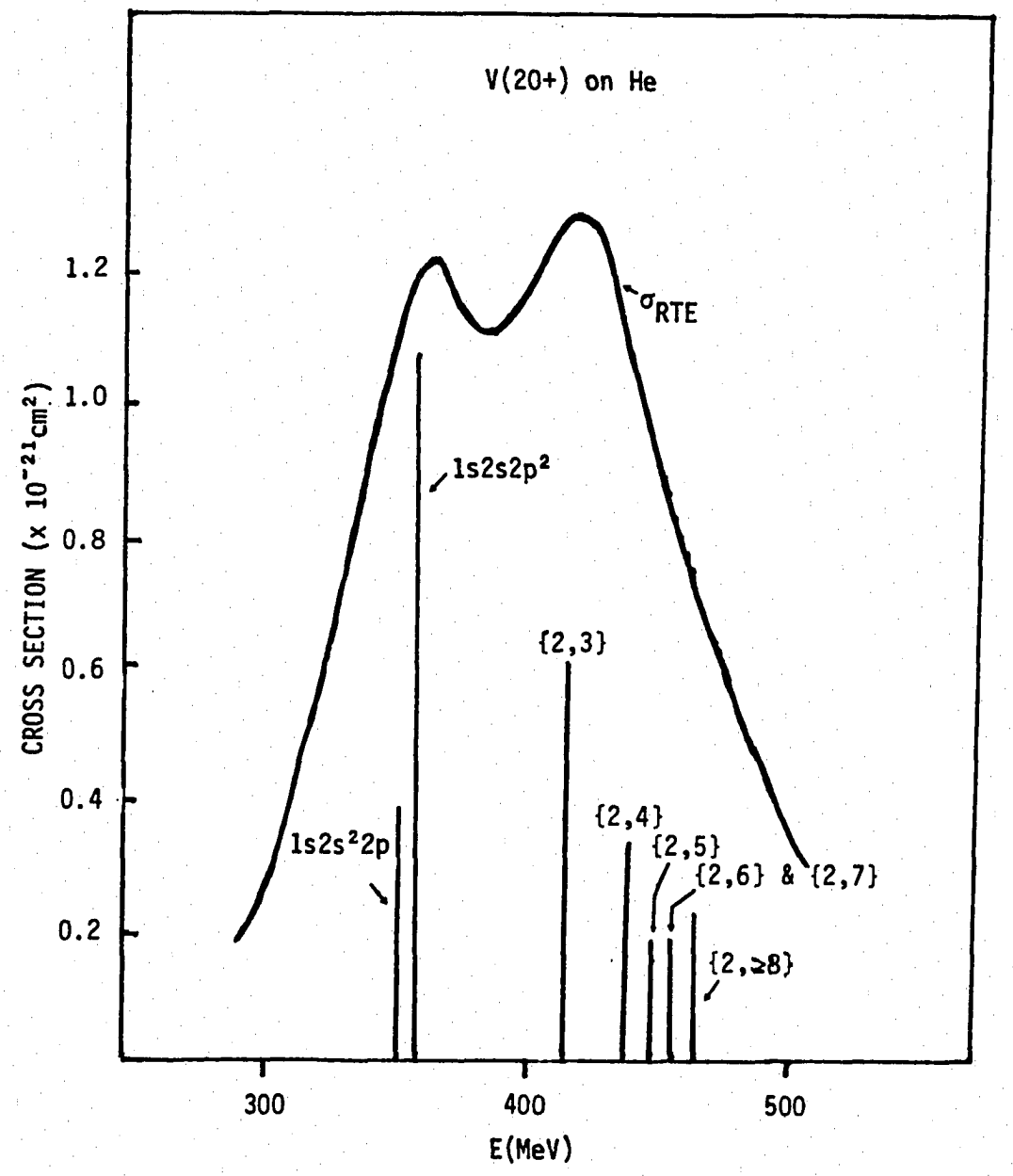

Figure 12. Calculated RTE cross section curve for V(20+) + He vs. projectile energy showing V(20+) DR cross sections. As before, numbers in brackets indicate the principal quantum numbers of the electrons participating in the formation of the resonance state.

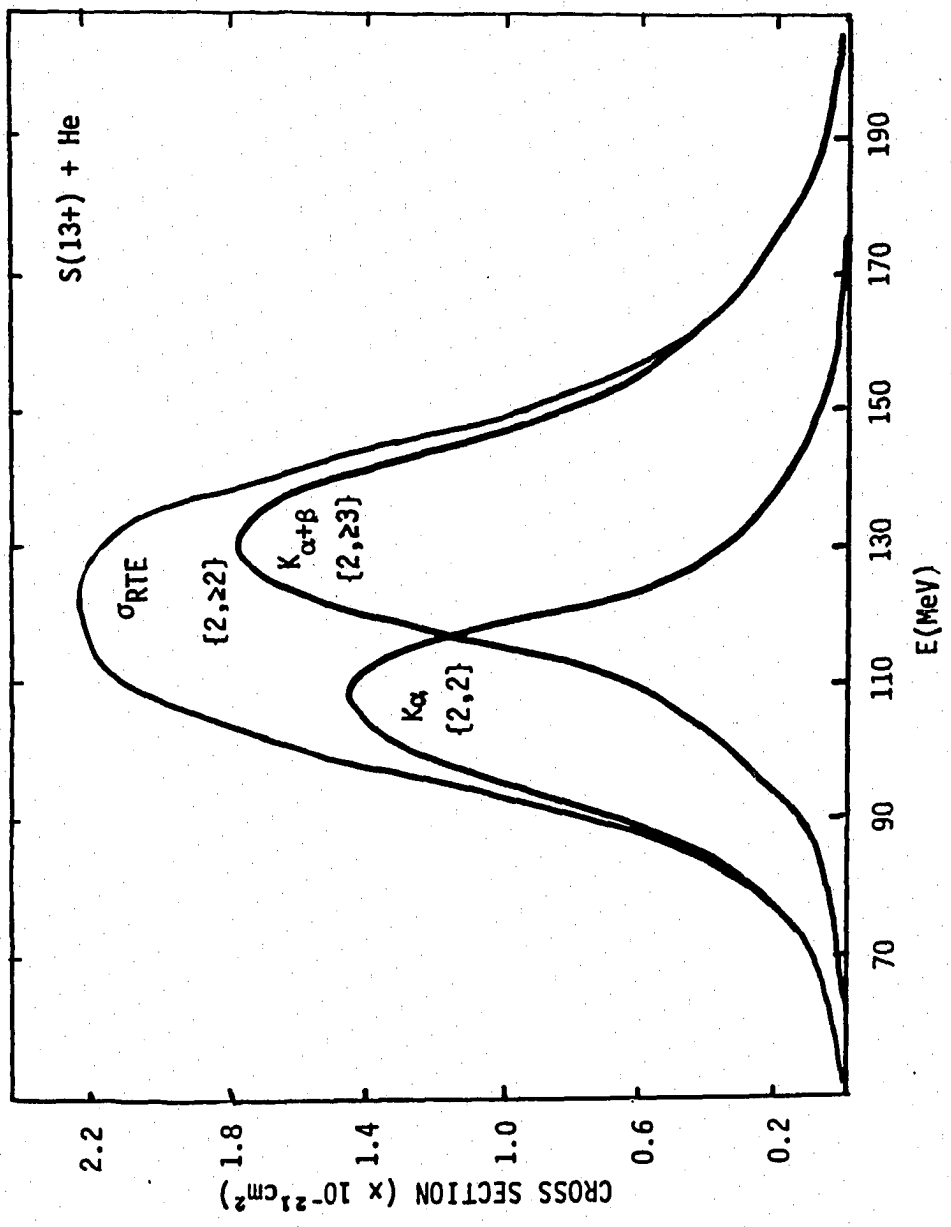

Figure 13. Contributions of {2,2} and {2,≥3} excited states to calculated RTE cross section for S(13+) on He.

calculated RTE cross section has been separated from the {2,≥3} contribution for S(13+) on He. More will be said about this in Chapter 5, Section 3.

It was stated earlier that some target electrons may not satisfy the impulse approximation. An inner electron in a high Z target may have a velocity which is comparable to the projectile ion velocity and should therefore be excluded from the calculation. This option has been included in OPUS3 so that it is also possible to separate the individual $\Psi_{n,l}$ subshells of the target and view their contributions to σ_{RTE} independently. Figure 14 is an example of such a calculation, carried out on the S(13+) + Ar system. It should be viewed in conjunction with the corresponding Ar Compton profile (Fig. 9b). The 1s electrons of Ar, which do not satisfy the impulse approximation, contribute only 2% to the total RTE cross section curve at the maximum.

The results of the calculations which pertain to the experiments to be discussed will be reexamined in the comparison of theory and experiment in Chapter IV.

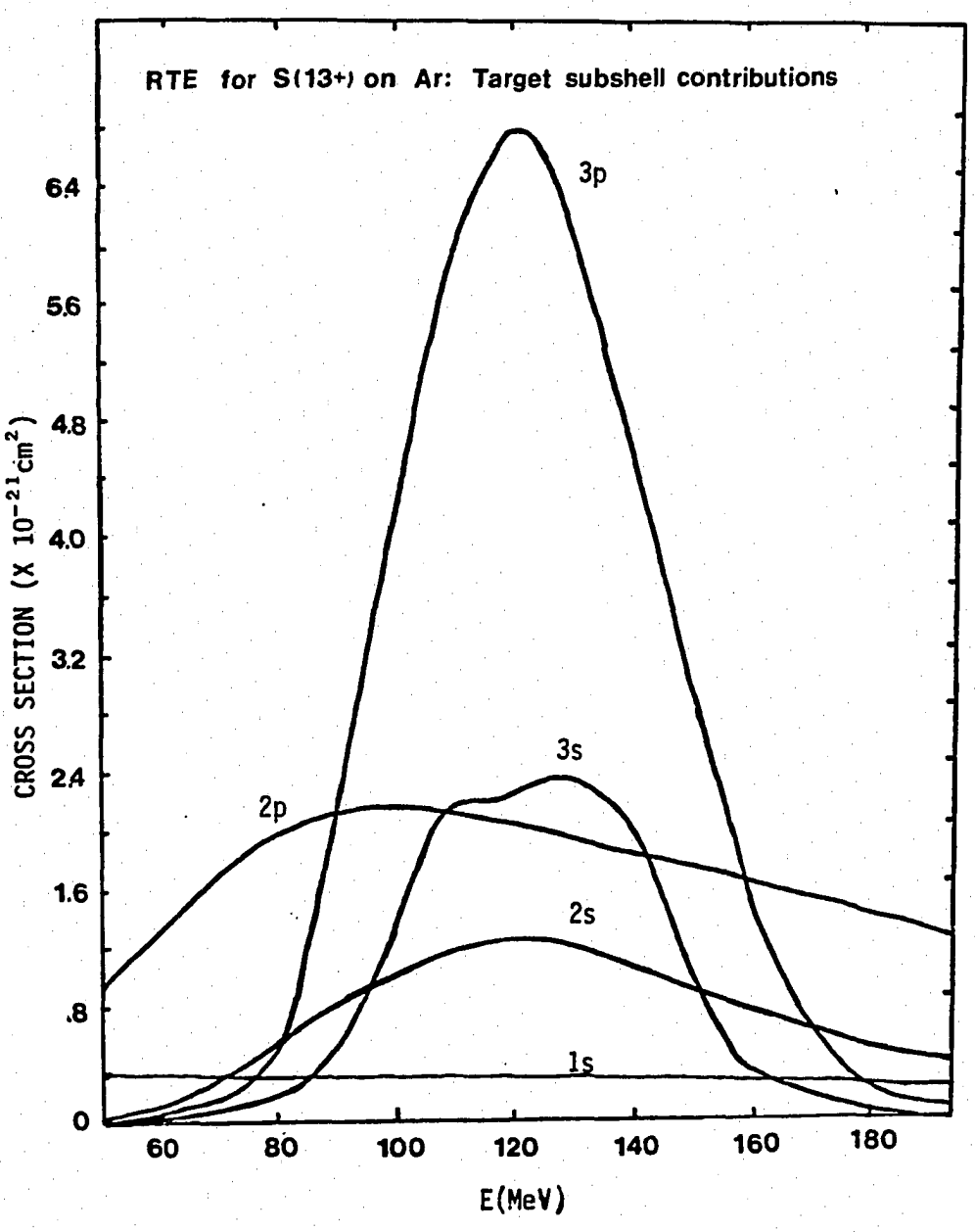

Figure 14. Contributions of individual target subshells to calculated RTE cross section for S(13+) + Ar.

CHAPTER IV

RESONANT-TRANSFER-AND-EXCITATION: EXPERIMENT

General

The RTE experiment to be discussed involves Li-like sulfur, S(13+), as a projectile incident on a He gas target, and was conducted at the Tandem Van de Graaff facility of the Brookhaven National Laboratory. The author participated in this experiment in collaboration with researchers from several Universities, the United States Department of Energy, and Brookhaven National Laboratories (Bernstein et al., 1984). The results and discussion section will not be limited to this experiment, however. The results of two very similar experiments (Tanis et al., 1984 and Tanis et al., in press) will also be considered for comparison to theoretical calculations. A brief description of an RTE experiment in general, without regard to the specific projectile/target system under study, precedes the discussion of the S(13+) on He experiment.

A projectile beam composed of highly charged ions is accelerated toward a gas cell containing the neutral target atoms. As the projectile speeds through the target chamber, it may interact with a target atom and form the intermediate resonance state which is characteristic of RTE. The excited state can then decay by x-ray emission. Since the formation of this state requires the transfer of an electron from the target atom to the projectile ion, the projectile ion which

has undergone capture can be distinguished from one which has not by electrostatic or magnetic separation of the charge-changed component of the projectile beam. Collecting the charge-changed component and the non-charge-changed component allows for determination of the fraction of projectiles which have captured an electron. But capture alone does not imply the occurrence of an RTE event. In order to determine that the intermediate excited state of interest has been formed, we must also detect the x ray which was given off back in the target chamber. A resonant behavior in the probability for these simultaneous events at the energy predicted by theory would be indicative of RTE.

A beam line which is designed to investigate and detect simultaneous capture and excitation must contain the following devices: slits to collimate the beam of projectiles, a target gas cell with an x-ray detector viewing the interaction region, an electrostatic or magnetic deflection mechanism to separate the outgoing charge states, particle detectors for each of the charge-changed beam components to be monitored, and a Faraday cup to collect the main beam. A schematic of the set-up which was used at Brookhaven is represented by Figure 15.

The essential feature of the electronics for an RTE experiment (See Fig. 16) is the ability to detect coincidence events. This is performed by a Time-to-Amplitude-Converter (TAC), which only outputs a signal if a particle and an x ray are observed within a preset short time period. The x-ray pulse from the Si(Li) detector is routed through a Timing Filter Amplifier (TFA) and a Constant Fraction Discriminator (CFD), which converts the analog signal (which is proportional

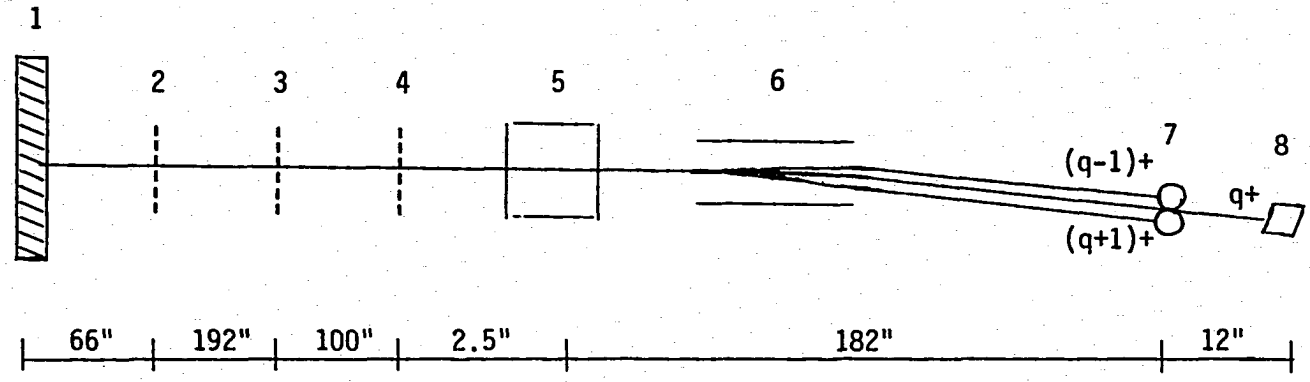

Figure 15. Schematic of beam line for S(13+) on He experiment.

Components shown:

1 wall
2 first slit
3 second slit
4 third slit
5 target cell and Si(Li) detector
6 electrostatic deflection plates
7 SB detectors
8 Faraday cup

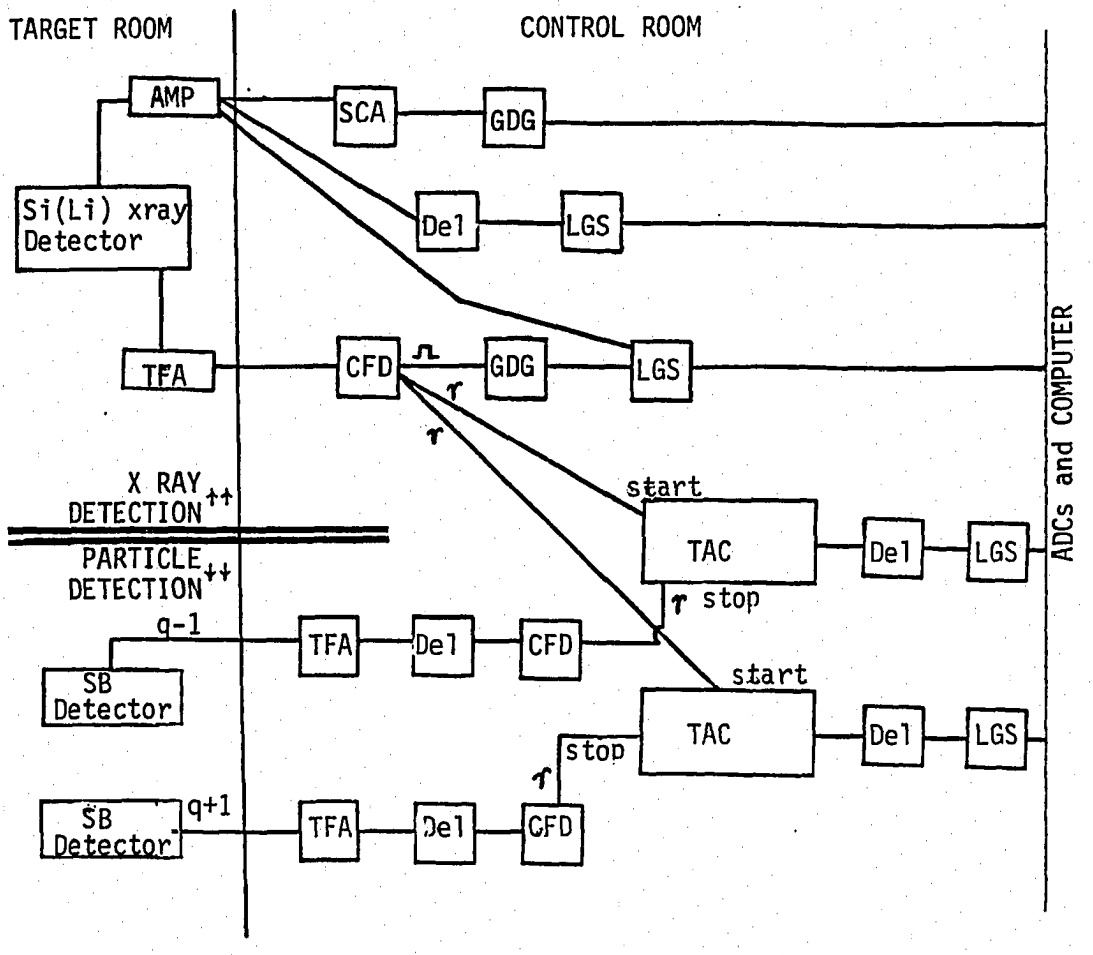

Figure 16. Schematic of beam line electronics for S(13+) + He experiment.

Key to abbreviations

TFA - Timing Filter Amplifier
SCA - Single Channel Analyzer
GDG - Gate and Delay Generator
LGS - Linear Gate Stretcher
CFD - Constant Fraction Discriminator
TAC - Time-to-Amplitude Converter
ADC - Analog/Digital Converter
Del - Timing Delay

to the amplitude of the x-ray pulse) into a logic signal if the amplitude exceeds the minimum setting on the discriminator. The logic signal from the CFD is the START signal for the TAC. A similar set of electronics from the particle detectors provides the STOP signal for the TAC. The TAC then outputs an analog pulse whose amplitude is proportional to the time difference between the START and STOP signals. The delay in the particle channel is adjusted to provide the necessary time difference between the START and STOP. After each TAC output, both x-ray and particle gates are closed until the next x ray of sufficient energy is observed. X rays are also directly monitored. The electronics diagram shown in Figure 16 represents the set-up used in the S(13+) and He experiment, and gives a general indication of the electronics requirements.

Each run is performed at a well-defined target cell gas pressure, as measured with a capacitance manometer, and several pressure runs are performed to test for linearity at each projectile energy value of interest. Collected at each energy and pressure are the following: total x rays, x rays in coincidence with particles, and particle counts for each of the analyzed beam components.

The S(13+) on He Experiment

In the representative experiment, measurements were made of single electron capture (q-1) and loss (q+1) in coincidence with sulfur K x-ray emission for 70-160 MeV S(13+) ions incident on He. A capacitance manometer was used to measure the gas cell pressure which, in all cases, was less than 60 microns (1 μ = 1 micron = 1 x 10^{-3} torr).

In the range studied, particle, x-ray, and coincidence counts varied linearly with pressure, indicating single collision conditions (Figs. 17a, b, and c). The projectile beam was collimated by two 1 mm^2 apertures roughly 2.5m apart before entering the differentially pumped target region (Fig. 15). An additional 3.6 mm^2 aperture to eliminate slit-scattered sulfur ions was placed just upstream of the target cell. Sulfur x rays were detected by a 200 mm^2 Si(Li) detector positioned at an angle of 90 degrees to the incident beam axis and about 4.8 mm away. The emerging capture and loss beams were electrostatically separated from the main beam and collected in surface barrier (SB) detectors. The main beam component (no charge change) was collected in a Faraday cup located behind the SB detectors and connected to a Keithley current integrator. Coincidences between sulfur K x rays and single electron capture and loss events were recorded with Time-to-Amplitude Converters (TACs) with a time resolution of about 50 nanoseconds. Total x-ray emission by the S ions was also recorded. Figures 18a and b show a typical Sulfur x-ray spectrum and a typical TAC spectrum. The computer in use at Brookhaven's Van de Graaff facility is a Xerox Sigma 7.

Cross sections were obtained as described below. A complete sample calculation of all cross sections of interest for one beam energy appears in Appendix B. Cross section uncertainties are based on the standard error in the slope resulting from a linear least squares fit to the fraction vs. pressure plots (see Fig. 17). Solid angle calculations and detector efficiencies were performed by M. Clark (private communication, December, 1983).

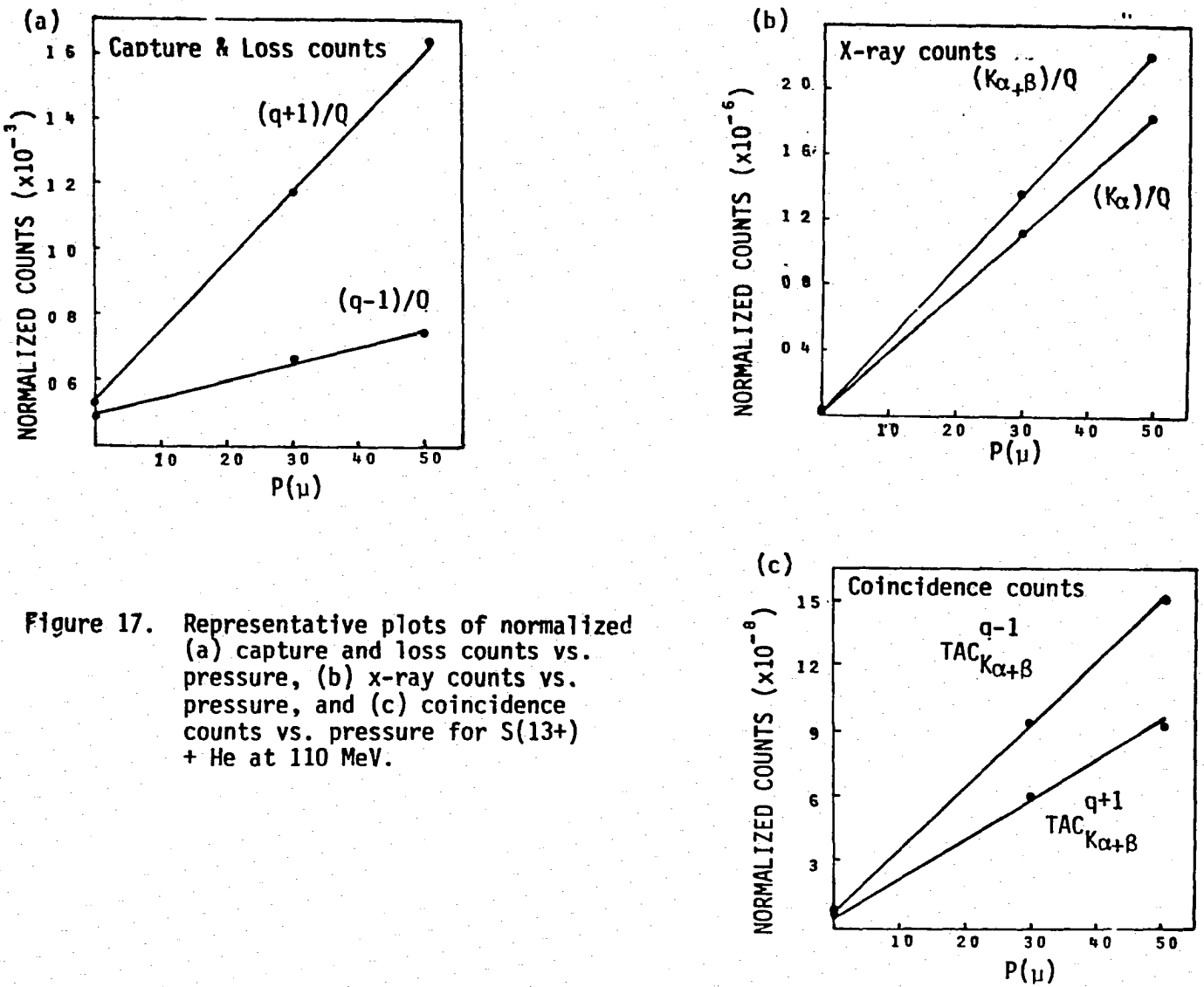

Figure 17. Representative plots of normalized (a) capture and loss counts vs. pressure, (b) x-ray counts vs. pressure, and (c) coincidence counts vs. pressure for S(13+) + He at 110 MeV.

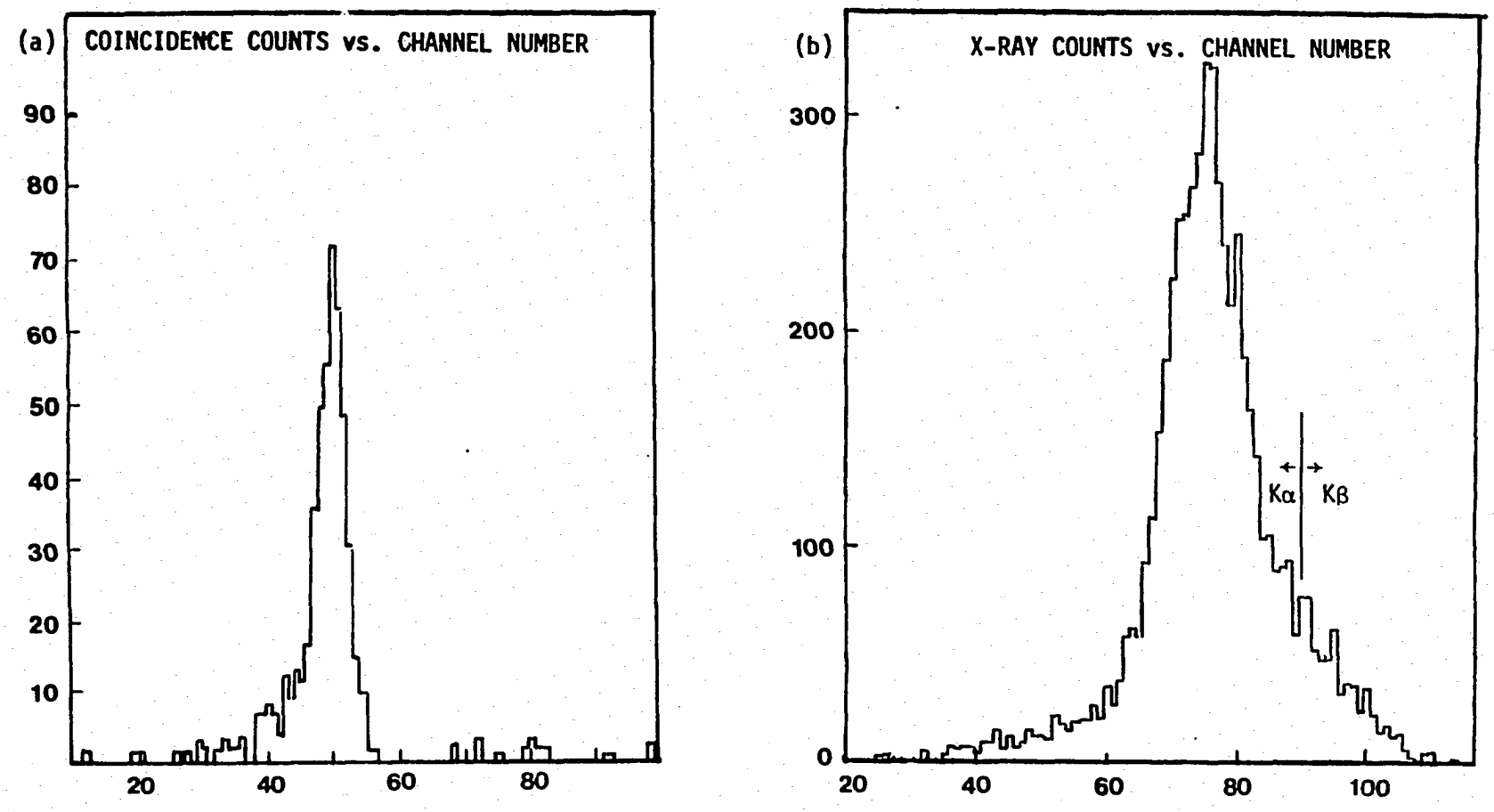

Figure 18. Representative computer plots of (a) coincidence counts vs. channel number and (b) x-ray counts vs. channel number for S(13+) + He experiment. X-ray counts for Kα and Kβ x rays obtained by summing over channels to the left (for Kα) of the vertical line and to the right (for Kβ) of the vertical line in figure 18b.

Determination of Cross Sections

The number of x rays, N_x, which were detected in the experiment as described, is dependent upon the geometry of the target cell, the incident beam intensity, I_o, the cross section for x-ray production, σ_x, the x-ray detector efficiency, ε_x, and the solid angle subtended by the detector as follows:

$$N_x = I_o \cdot \sigma_x \cdot \varepsilon_x \cdot (\Delta\Omega_x/4\pi) \cdot (N\ell P) \tag{4.1}$$

The quantity (NℓP) is the thickness of the target cell, where $N=3.3\times10^{13}$ at/cm$^3\mu$, ℓ is the target cell length in cm, and P is the pressure in microns. The fraction of x rays which are detected, F_x, is obtained by dividing equation (4.1) through by I_o,

$$F_x = \frac{N_x}{I_o} = \sigma_x \cdot \varepsilon_x \cdot (\Delta\Omega_x/4\pi) \cdot (N\ell P). \tag{4.2}$$

If the fraction F_x depends linearly on P, then

$$\frac{\Delta F_x}{\Delta P} = \sigma_x \cdot \varepsilon_x \cdot (\Delta\Omega_x/4\pi) \cdot (N\ell). \tag{4.3}$$

The cross section for x-ray production then, is given by

$$\sigma_x = \{4\pi/(\varepsilon_x \cdot \Delta\Omega_x \cdot N\ell)\} \cdot \frac{\Delta F_x}{\Delta P} \tag{4.4}$$

All cross sections of interest can be calculated in this manner, since the plots of all particle or x-ray counts are linear with pressure (see Fig. 17 for examples) under single collision conditions. For

generality, equation (4.4) is simplified to

$$\sigma_i = C_i \cdot \frac{\Delta F_i}{\Delta P} \tag{4.5}$$

where the subscript, i, represents the species understudy. The constant C_i varies depending upon the species. For x rays and x rays in coincidence with charge changing events, C_i is given by the term in brackets in equation (4.4), where ε_x differs depending upon which x rays ($K\alpha$, $K\beta$, or $K\alpha_{+}\beta$) are involved in the cross section under study. For capture and loss cross sections,

$$C_{q,q\pm1} = \frac{1}{N \cdot \ell} \tag{4.6}$$

since $\Delta\Omega_x = 4\pi$ and $\varepsilon_x = 1$.

CHAPTER V

RESULTS AND DISCUSSION

S(13+) on He

The results obtained from the experimental data are presented in the following three figures. Figures 19a and b represent the cross sections for capture and loss of one electron in coincidence with x-ray emission, $\sigma_X^{q\pm1}$. The charge-changing events coincident with K_α x rays have been separated from the total K x-ray yield, and are represented by the curves labled $\sigma_{K\alpha}^{q\pm1}$ and $\sigma_{K(\alpha+\beta)}^{q\pm1}$, respectively. The electron loss curve (Fig. 19b) is nearly independent of projectile energy. The cross section for coincident capture and x-ray emission, $\sigma_{K(\alpha+\beta)}^{q-1}$, exhibits a large peak with a maximum around 125 or 130 MeV. This cross section is due to all simultaneous capture and excitation events whether due to RTE or NTE. The NTE contribution, as discussed in Chapter II, is assumed to be no larger than the background at the low energy side of the resonant peak, which contributes 14% to the maximum at 130 MeV. It is asserted that the peak which lies above the background is attributable to Resonant-Transfer-and-Excitation.

On figure 19a, the RTE curve which represents electron capture with emission of K_α x rays only, $\sigma_{K\alpha}^{q-1}$, is equal to the cross section for all q-1 TAC events, $\sigma_{K(\alpha+\beta)}^{q-1}$, within the limit of error for energies between 70 and 110 MeV. Thus, it can be cautiously asserted that no RTE events in that energy range result in K_β x rays. This is consistent with the selective formation of excited states which can yield only

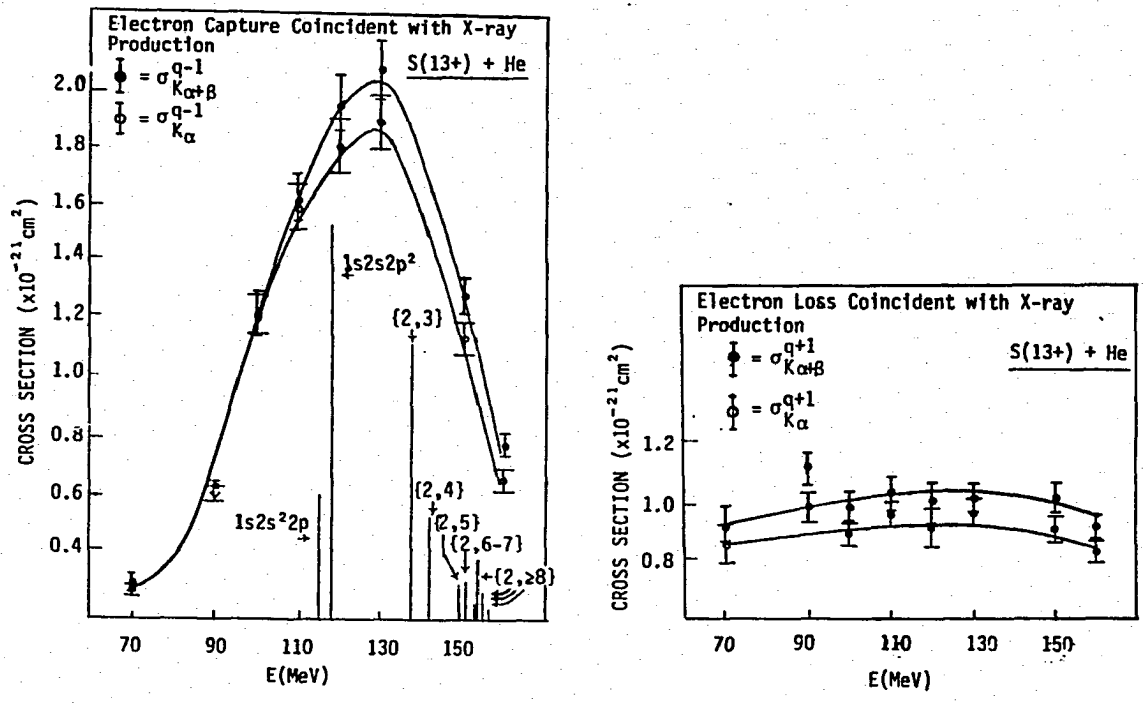

Figure 19. Cross sections for simultaneous charge changing and x-ray emission events vs. projectile energy for S(13+) + He: (a) electron capture with x-ray emission (RTE and NTE) and (b) electron loss with x-ray emission. Curves are drawn to guide the eye. Numbers in brackets on electron capture curve represent principal quantum numbers of electrons participating in formation of excited state characteristic of DR and RTE. Spikes below RTE curve represent cross sections for DR for S(13+) from McLaughlin and Hahn (1982), Table 1.

K_α x rays, i.e., in the energy range of the {2,2} excited states (Chapters II and III). The DR transition energies, transformed to projectile ion energies, appear as spikes below the RTE curve.

The total x-ray production cross sections are given in Figure 20a, where the cross section for total x rays, $\sigma_{K(\alpha+\beta)}$, has been separated from the cross section for K_α x rays, $\sigma_{K\alpha}$. This shows that K_β x rays are emitted in the resonant region even though they are not detected in coincidence with electron capture. Hence, they result most probably from excitation events (no projectile charge change), as do the K_α events which are not associated with capture.

Included in Figure 20b is the ratio of K_α x-ray counts to $K_{(\alpha+\beta)}$ x ray counts, both in coincidence with electron capture. The number of counts were summed over all pressures greater than zero. These measurements are independent of geometry, and again show that incident energies corresponding to {2,2} transitions give rise only to K_α x rays (within the error margin) since the ratio is approximately one for 90 to 110 MeV and drops off with increasing projectile energy. Any K_β x rays produced at energies in the range of 90 to 110 MeV are presumed to result from NTE events. The high energy decline is attributed to RTE with K_β emission from the intermediate excited states $\{2,\geq 3\}$.

Figure 21 shows the electron capture and loss cross sections, $\sigma_{q,q\pm1}$, calculated from the average of the long time runs used to collect coincidence events at high counting rates, and the short time (10 or 20 seconds) runs at low counting rates which were performed for each energy as a check on the linear pressure dependence of the long time runs. The capture cross section shows the expected decreasing

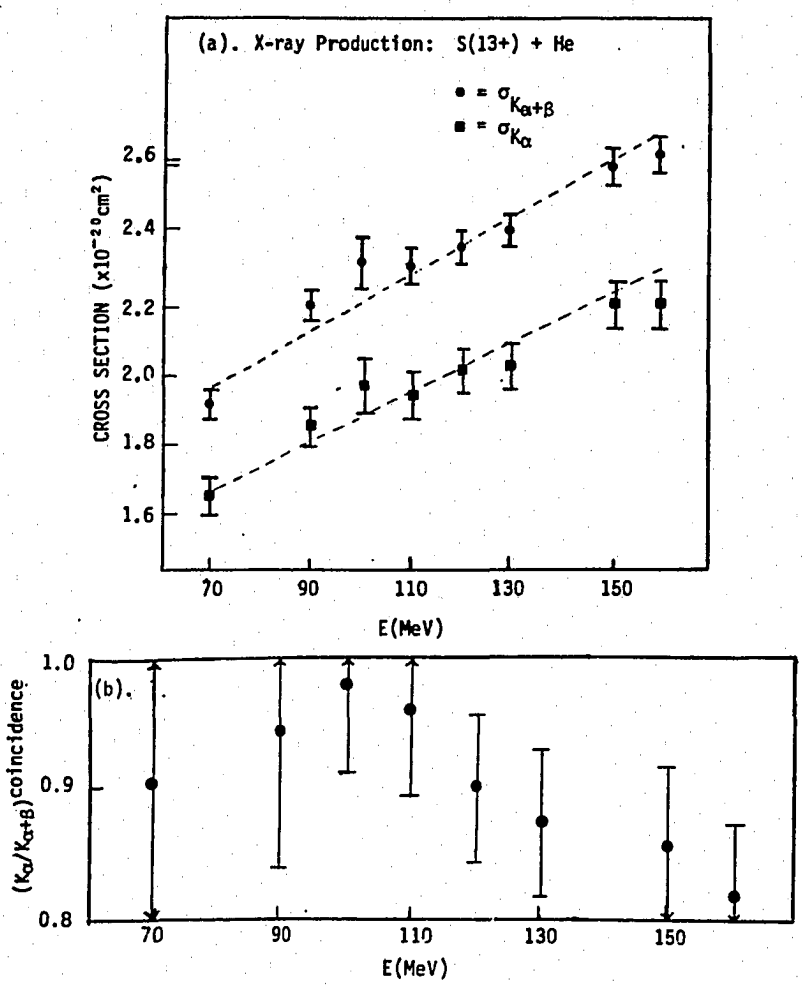

Figure 20. (a). X-ray production cross sections vs. projectile energy for S(13+) + He. Total x rays have been separated from Kα x rays. Lines are drawn to guide the eye. (b). Ratio of Kα coincidence counts to Kα+β coincidence counts vs. projectile energy for S(13+) + He. Counting errors are shown.

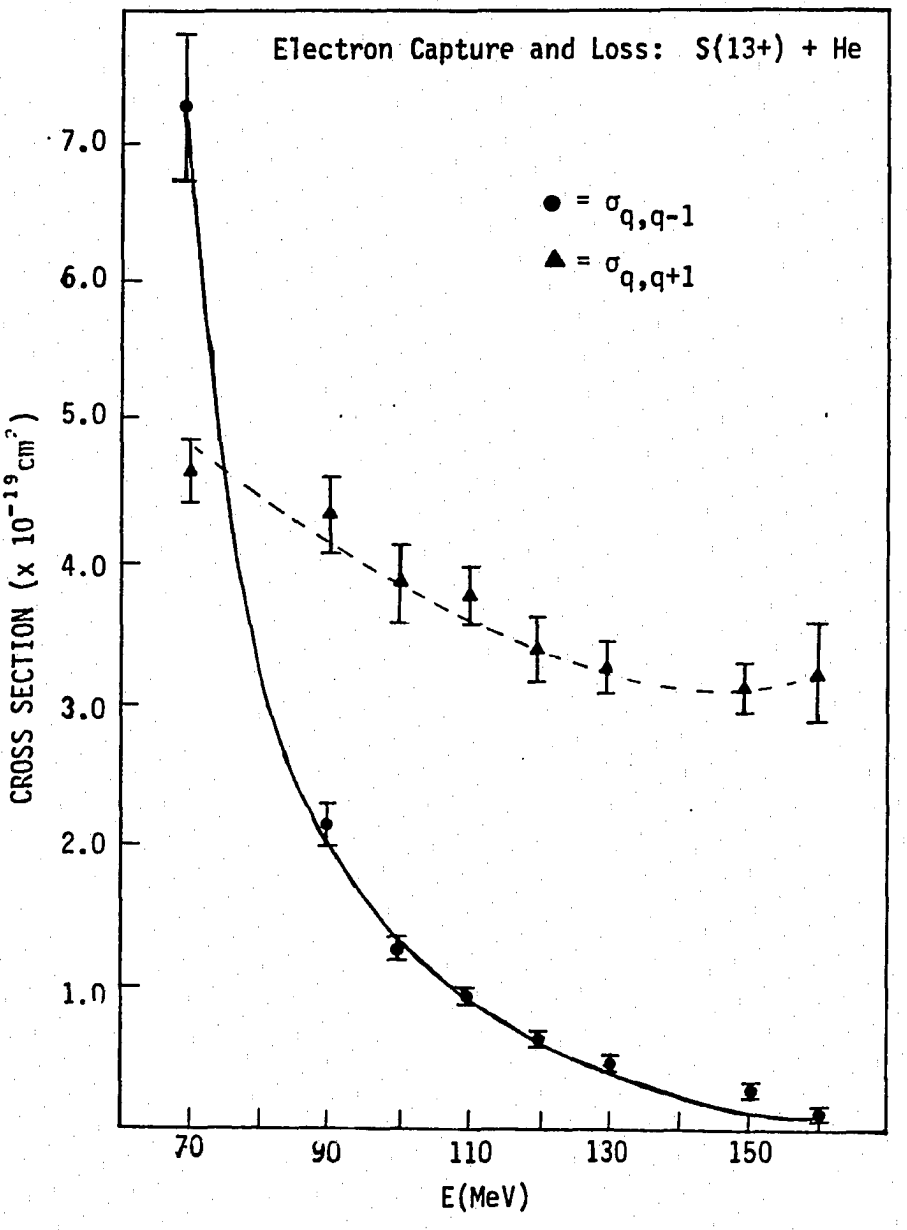

Figure 21. Electron capture and loss cross sections vs. projectile energy for S(13+) + He. Lines are drawn to guide the eye.

exponential behavior (Chapter II).

Other Experiments

Two similar RTE experiments (Tanis et al., 1984 and Tanis et al., in press), both using He as a target, have been performed. In one case, the projectile was Ca(17+) and in the other V(20+). Both experiments were performed on the SuperHILAC accelerator at the Lawrence Berkeley Laboratory. The experimental set-ups were similar to that which has been described above for S(13+) on He at Brookhaven. Some additional information involving other incident and outgoing charge states was obtained, but since this thesis is restricted to discussion of Li-like ions on He with single electron capture, we will consider the relevant portions of these experiments. Results of all three experiments are discussed and compared with theory in the following section.

Comparison of Experiment and Theory

Figures 22, 23 and 24 show the results of the three experiments mentioned and the corresponding theoretical RTE curves which were discussed in Chapter III. The DR cross sections for S(13+) and V(20+) were calculated by McLaughlin and Hahn (1982) and Nasser and Hahn (1983), respectively. The DR cross sections sections for Ca(17+) were obtained by interpolation of these data. The energies of the DR peaks for Ca and V were scaled from S by the square of the atomic number (eqn. 3.4) and then transformed to the lab projectile energy (eqn. 3.3).

With regard first to the S(13+) experiment (Fig. 22), transitions resulting from the formation of the particular resonance states and

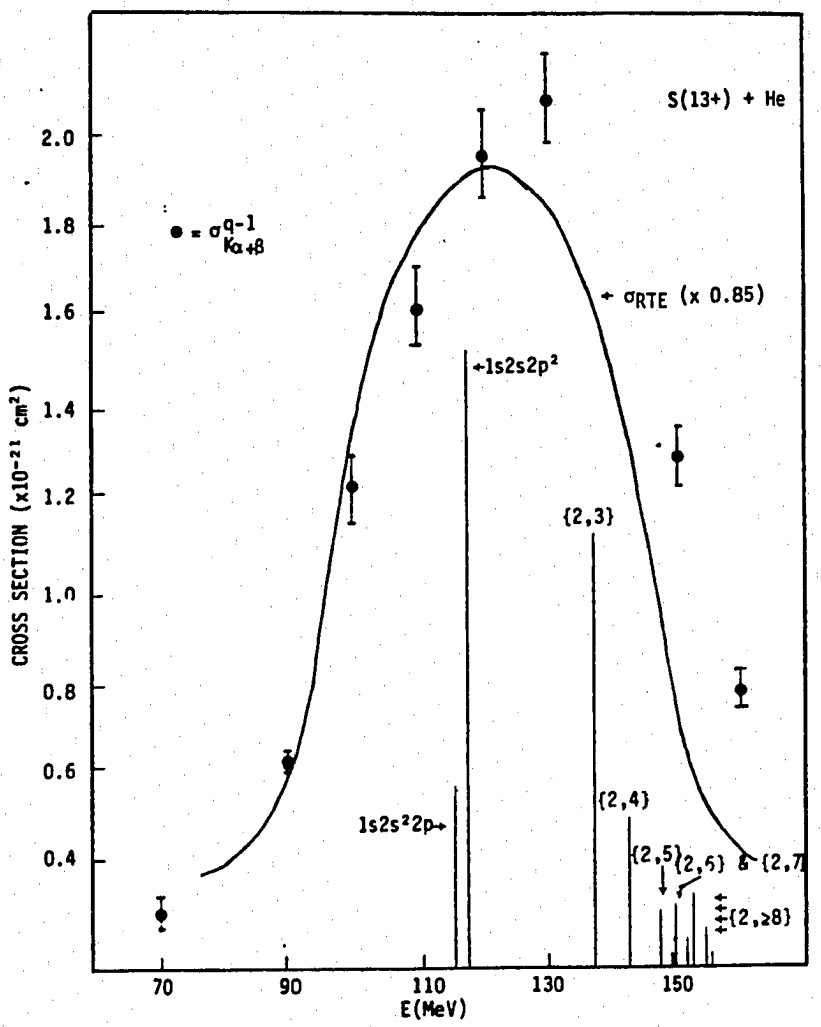

Figure 22. Calculated and experimental RTE cross sections for S(13+) + He as functions of projectile energy. Calculated cross sections scaled to emphasize agreement in lineshape. Spikes below calculated RTE curve represent DR cross sections for S(13+) transformed to lab frame energies (McLaughlin and Hahn,1982, see Figure 4 and Table 1). Numbers in brackets represent principal quantum numbers of electrons participating in formation of resonance state.

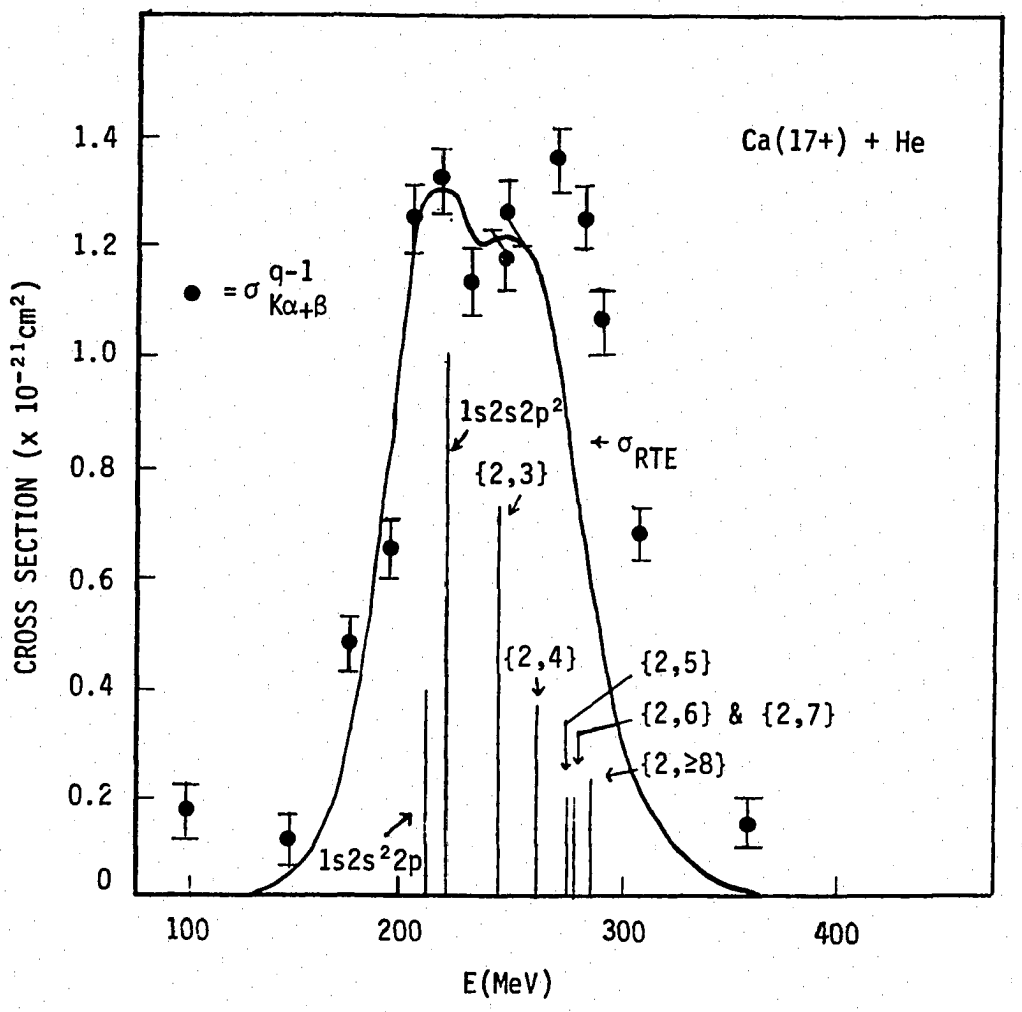

Figure 23. Calculated and experimental RTE cross sections for Ca(17+) + He as functions of projectile energy. Calculated cross section scaled to emphasize agreement in lineshape. Spikes below calculated RTE curve represent DR cross sections for Ca(17+) transformed to lab frame energies. Scaling of the relative magnitudes of the DR cross sections for Ca(17+) obtained by interpolation of Nassar and Hahn's (1983) data. Numbers in brackets represent principal quantum numbers of electrons participating in the formation of the resonance state.

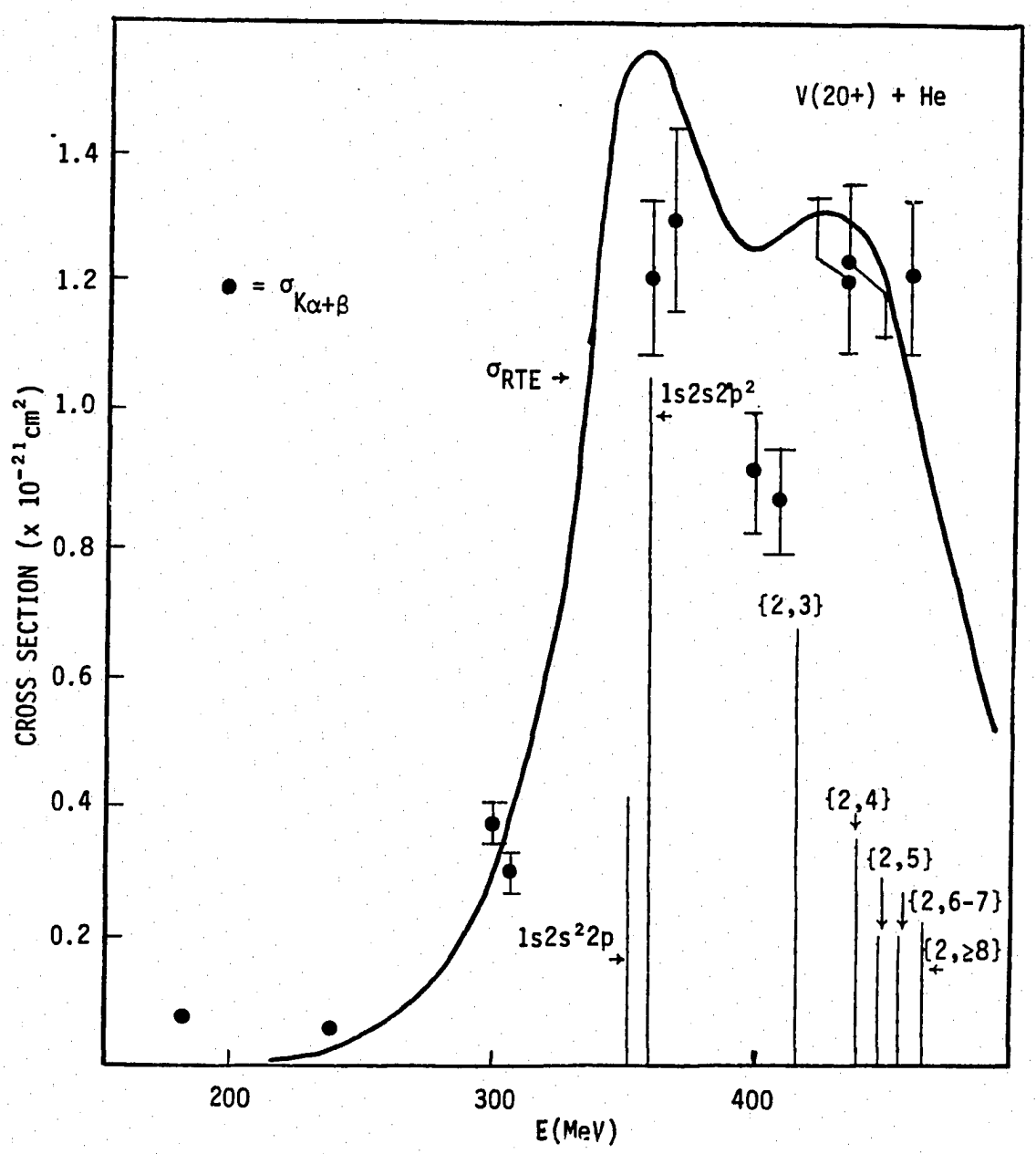

Figure 24. Calculated and experimental RTE cross sections for V(20+) + He as functions of projectile energy. Calculated cross sections scaled to emphasize agreement in lineshape. Spikes below calculated RTE curve represent DR cross sections for V(20+) transformed to lab frame energy. Relative magnitudes of DR cross sections from Hassar and Hahn (1983). Numbers in brackets represent principal quantum numbers of electrons participating in the formation of the resonance state.

their relation to the experimental RTE events yielding either K_α or K_β x rays have been discussed in the first section of this chapter. The correspondence between theory and experiment is now the salient point. The theoretical and experimental maxima appear only 5 MeV apart, and there is general correspondence between the shapes of the two curves. Comparison of the peak heights will be made later.

In Figure 23, representing Ca(17+) on He, the doubly-peaked structure predicted by theory appears. Recall from Chapter III that the two peaks represent the two groups of resonance states, {2,2} and {2,≥3}, which can be formed. Though the correspondence between the first peaks is good, the second peak in the experimental cross section appears at about 40 MeV above that which was predicted. Also, the experimental minimum between the two maxima is deeper than the theoretical minimum.

Figure 24 displays the results of the V(20+) experiment. Here again, the predicted structure emerges, and the positions of the theoretical and experimental low energy maxima coincide. As with Ca(17+), a discrepancy appears in the relative depth of the minimum.

Consider first the relative position of the second maximum of the Ca cross section, and the depth of the minima which appear between the two peaks for both Ca and V. In the calculation, the second peak is due to the group of intermediate resonance states, {2,≥3} in the DR cross section calculation (Table 1). There are at least four possible sets of circumstances which would alleviate one or both of the difficulties. All involve modification of the calculated RTE cross sections.

The first consideration is that the Compton profile for the target may be too broad. While this would lower the theoretical minimum, there would be no corresponding increase in the energy of the second peak, and the agreement in the rise of the first peak would suffer. Secondly, the Auger energies of the {2,≥3} states in the DR data may be too low. Both difficulties, the depth of the minimum and the position of the second peak, would be resolved if this were the case. The DR transition energies were uniformly scaled by the ratio of the squares of the atomic numbers (eqn. 3.4), which is an approximation, and so these energies may not represent the Auger energies of the excited states exactly. An increase in the relative heights of the transitions (DR cross sections) which occur at higher energies would give better agreement to the experimental energy, but it wouldn't help the "dip". The fourth possibility is that the transitions {≥3,≥3}, which do not appear in the calculated DR cross sections of Nasser and Hahn (1983), McLaughlin and Hahn (1982), and Hahn (personal communication, October 3, 1983) would occur at energies either comparable to or higher than the {2,≥3} group, and would therefore have the effect of shifting the position of the second peak to higher energy. This would not, however, alleviate the difficulty with the minimum between the two peaks, unless the {2,3} DR transition was found to have a smaller cross section than that which was used. Any of the last three possibilities could also account for the fact that the experimental maximum in the S(13+) cross section occurs at slightly higher energy than the theoretical. Whether any or all of the situations mentioned give rise to the observed discrepancies between theory and experiment requires further study.

The agreement between the low energy rise and position of the S(13+) peak and the first peak in the Ca(17+) and V(20+) experiments with theory indicates that the calculated DR transition energies and magnitudes for the {2,2} transitions are consistent with what is observed experimentally. Furthermore, if the calculated magnitudes of these peaks are compared to the magnitudes of the experimental peaks, the difference, $\sigma_{theor} - \sigma_{exp}$, is nearly constant and equal to 0.4×10^{-21} cm^2 (Fig. 25). This result is encouraging, but stated cautiously, since the overall absolute error in any of these experiments could be a large as 30%. The shape of the cross sections would be unaffected by such an error, but the magnitude could be shifted to a higher or lower cross section value as a result.

Despite the discrepancies with theory mentioned above, the overall agreement in low energy peak positions, the fact that both theory and experiment result in the doubly-peaked structure for heavier projectiles and the agreement in the absolute magnitudes of the first peaks, leads one to believe that the RTE model of Brandt (1983a) and the DR cross section calculations of Nassar and Hahn (1983), McLaughlin and Hahn (1982) and Hahn (personal communication, October 3, 1983) are applicable to the experimental results presented here.

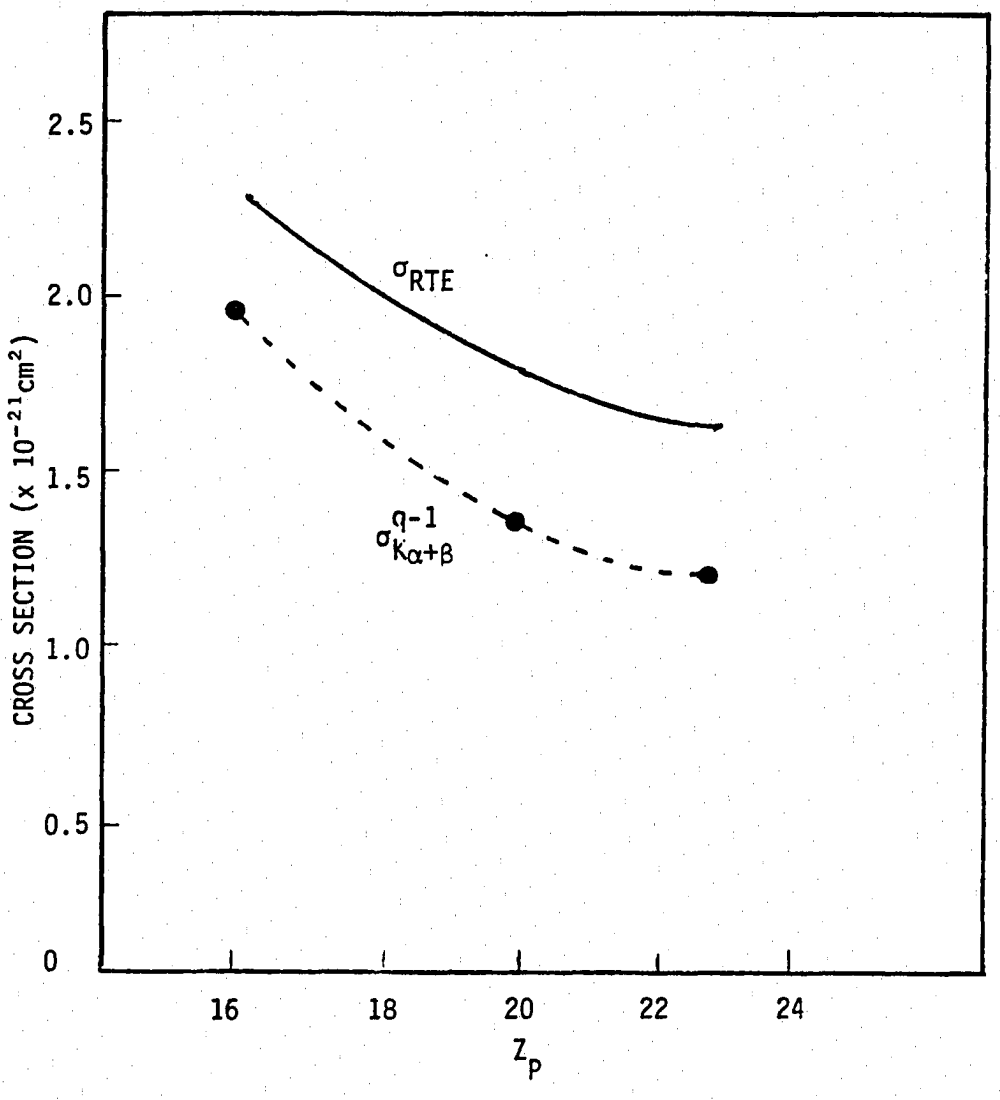

Figure 25. Comparison of calculated and experimental low energy RTE peak magnitudes for S(13+), Ca(17+), and V(20+) ions incident on He. The line through $\sigma_{K\alpha+\beta}$ is drawn to guide the eye.

CHAPTER VI

CONCLUSION

The experiment studied in this work, the two additional studies cited, and other experimental investigations of RTE, have lent credence to the actual existence of the process of RTE as described. The question which this work has attempted to address is whether there exists a close relationship between DR and RTE, since the theory which has been compared to experimental work is based upon DR cross sections. If the relationship could be shown, then aside from scientific curiosity, a major justification for further study of RTE would be the acquisition of knowledge concerning DR. Since DR is important in fusion plasmas both on earth and in the stars, study of RTE could conceivably contribute to a more comprehensive understanding of some astrophysical and fusion related phenomena. Let us briefly review the evidence in support of the relationship.

The experimental observation of resonant behavior in the $\sigma^{q-1}_{K(\alpha+\beta)}$ cross section very near to the energies predicted by theory has been clearly demonstrated in the case of three different lithiumlike projectiles incident on He. The production of x rays of different energies (K_α and K_β) at different projectile energies as predicted by theory has been experimentally verified. In the case of "heavy" and "light" projectiles incident on He (a "light" target), we have seen structure and no structure, respectively, corresponding to groups of intermediate resonant states, as predicted. Tentatively, there exists

a quantitative relationship between the theoretical and experimental heights of the low energy peaks (resulting from the formation of the {2,2} resonance states) in the RTE cross sections for both Ca(17+) and V(20+). Furthermore, the rise of this peak in the experimental and theoretical curves is almost identical. The competing process of NTE has not appreciably interfered with the observation of the resonant process for the systems discussed. That there exist some discrepancies between the theory of Brandt (1983a) and the experiments implies that further refinements are required, and the interesting experimental prospects have by no means been exhausted. Future studies are planned, by the Western Michigan University atomic physics group and collaborators, to investigate projectile and target Z dependence, and projectile charge state dependence. Using the experimental RTE set-up as described, the NTE contribution can be verified. These studies will undoubtedly contribute to a more thorough understanding of RTE, NTE and DR.

Such comprehensive agreement with respect to the points mentioned above prompts one to assert that the theory upon which the calculations are based has some basis in observable fact, and that on the surface at least, there does exist an elegant and simple relationship between Dielectronic Recombination and Resonant-Transfer-and-Excitation.

APPENDIX A

OPUS3

The following pages constitute an exact copy of the program used to perform all of the theoretical RTE calculations which appear in this thesis. Additional capabilities of OPUS3 are described in Chapter III, Section 3.

```
00100    C
00200    C
00300    C ***** OPUS3
00400    C       WRITTEN BY CAROLLYN SLOAN OGLESBY
00500    C       UNDER THE DIRECTION OF J.A. TANIS AND E.M. BERNSTEIN
00600    C       AT WESTERN MICHIGAN UNIVERSITY
00700    C       THIS EDITION DATED JUNE 14, 1984
00800    C
00900    C ***** OPUS3 IS DESIGNED TO CALCULATE RESONANT TRANSFER AND
01000    C       EXCITATION CROSS SECTIONS ACCORDING TO THE THEORY OF
01100    C       DETLEV BRANDT (REF. 1)
01200    C
01300    C       THE CALCULATION REQUIRES DATA AS FOLLOWS:
01400    C       FOR THE PROJECTILE:
01500    C               DR CROSS-SECTIONS AND
01600    C               THE AUGER ENERGIES OF THE DR TRANSITIONS
01700    C               (REF. 2)
01800    C       FOR THE TARGET:
01900    C               THE COMPTON PROFILE (REF. 3)
02000    C
02100    C       THE CALCULATION CAN BE PERFORMED ON THE FOLLOWING:
02200    C       PROJECTILES:            DATA FILE:
02300    C               SILICON(+11)            FOR24.DAT
02400    C               SULFUR(+13)                 .
02500    C               ARGON(+15)                  .
02600    C               CALCIUM(+17)                .
02700    C               SCANDIUM(+18)               .
02800    C               TITANIUM(+19)               .
02900    C               VANADIUM(+20)               .
03000    C               IRON(+23)                   .
03100    C       TARGETS:                DATA FILE:
03200    C               HYDROGEN                FOR26.DAT
03300    C               HELIUM                  FOR22.DAT
03400    C               NEON                    FOR21.DAT
03500    C               ARGON                   FOR20.DAT
03600    C               XENON                   FOR28.DAT
03700    C
03800    C
03900    C ***** PRELIMINARIES TO EXECUTION ************ HAVING TROUBLE?
03901    C                                                   DID YOU DO THIS?
04000    C       ** FOR SILICON(+11) PROJECTILE - TYPE WHILE IN MONITOR
04100    C         .COPY FOR24.DAT=SIP.DAT
04200    C       ** FOR ANY OTHER PROJECTILE - TYPE WHILE IN MONITOR
04300    C         .COPY FOR24.DAT=SP.DAT
04400    C
04500    C       THE PROGRAM IS INTERACTIVE AS WRITTEN, AND WILL
04600    C       PROMPT ALL REQUIRED INFORMATION FROM THE OPERATOR.
04700    C       PAY SPECIAL ATTENTION TO THE INPUT FORMAT.
04800    C       ALL OTHER DATA REQUIRED IS AUTOMATICALLY READ
04900    C       BY FOROTS.  THIS MEANS THAT ALL REQUIRED DATA FILES
05000    C       APPEAR IN THE FORM 'FOR__.DAT'  THE DATA FILES IN
05100    C       THIS SUBFILE ARE REQUIRED FOR THE EXECUTION OF OPUS3.
05200    C
05300    C
05400    C ***** DEFINITIONS
05500    C       ARRAYS:
05600    C               DRER(21,2) - CONTAINS PROJECTILE INFORMATION
05700    C               DR CROSS-SECTIONS AND THEIR CORRESPONDING
05800    C               AUGER ENERGIES - READ FROM FOR24.DAT
05900    C
06000    C               QPIZ(31) - CONTAINS COMPTON PROFILE MOMENTUM
06100    C               ARGUMENT - SAME FOR ALL TARGETS - READ FROM
06200    C               FOR25.DAT
06300    C
06400    C               EPR(200) - CONTAINS PROJECTILE ENERGIES FOR
06500    C               ENERGY RANGE OF CALCULATION DESIRED - INTERNALLY
06600    C               GENERATED AFTER MINEN, MAXEN, AND MEEV ARE
06700    C               SUPPLIED.
06800    C
```

```
C
C          SPECT(200,2) - CONTAINS RTE CROSS-SECTIONS AND
C          CORRESPONDING PROJECTILE ENERGIES AFTER CAL-
C          CULATION - INTERNALLY GENERATED
C
C          CPJ(31,17) - THE MOMENTUM DISTRIBUTION OF THE
C          TARGET - READ FROM FOR__.DAT, WHERE __ = 20, 21,
C          22, 26, OR 28 AS ABOVE FOR THE TARGET OF CHOICE.
C
C          Y(17) - TEMPORARY ARRAY REQUIRED BY INTERPOLA-
C          TION ROUTINE.
C
C     VARIABLES
C         EXTERNAL (SUPPLIED BY OPERATOR)
C             NOPROJ = ATOMIC NUMBER OF PROJECTILE
C             NORB - DEFINES TARGET
C                  = 0 FOR HYDROGEN
C                  = 1 FOR HELIUM
C                  = 3 FOR NEON
C                  = 5 FOR ARGON
C                  = 17 FOR XENON
C               THE NUMBERS CORRESPOND TO THE NUMBER OF
C               COLUMNS IN THE COMPTON PROFILE - EXCEPTING
C               HYDROGEN, FOR WHICH VARIABLE NHY IS INTER-
C               NALLY DEFINED.
C             MIN - TELLS OPUS3 WHICH TARGET ELECTRONS TO
C                   INCLUDE (WHICH COLUMN IN COMPTON PROFILE
C                   STARTS SUM)
C                 = 1 INCLUDE ALL
C                 = 2 EXCLUDE 1S
C                 = 3 EXCLUDE 1S AND 2S
C                 = 5 EXCLUDE 1S, 2S, AND 2P
C
C             MINEN = MINIMUM PROJECTILE ENERGY IN MEV
C             MAXEN = MAXIMUM PROJECTILE ENERGY IN MEV
C             MEEV = STEP SIZE BETWEEN PROJECTILE ENERGY
C                    POINTS IN MEV
C             MYES - ALLOWS FOR MODIFICATION OF DR CROSS-SEC-
C                    TIONS IN PROJECTILE DATA FILE - FOR24.DAT
C                 = 0  NO MODIFICATION
C                 = 1  MODIFY ONE GROUP OF DR CROSS-SECTIONS
C                 = 2  MODIFY TWO GROUPS OF DR CROSS-SECTIONS
C               FOR MYES = 1  OPERATOR RECEIVES PROMPT FOR:
C                 MA = FIRST ROW OF FOR24.DAT TO BE MODIFIED
C                 MB = LAST ROW OF FOR24.DAT TO BE MODIFIED
C                 SCALE1 = NUMBER TO MULTIPLY DR CROSS-SEC-
C                          TIONS IN RANGE MA TO MB BY.
C               FOR MYES = 2  OPERATOR RECEIVES PROMPT FOR:
C                 MA = SEE ABOVE
C                 MB = SEE ABOVE
C                 SCALE1 = SEE ABOVE
C                 MC = FIRST ROW OF SECOND GROUP OF DR CROSS-
C                      SECTIONS IN FOR24.DAT TO BE MODIFIED
C                 MD = LAST ROW OF SECOND GROUP OF DR CROSS-
C                      SECTIONS IN FOR24.DAT TO BE MODIFIED
C                 SCALE2 = NUMBER TO MULTIPLY DR CROSS-SEC-
C                          TIONS IN RANGE MC TO MD BY.
C             MENGY - ALLOWS FOR MODIFICATION OF AUGER
C                     ENERGIES IN PROJECTILE DATA FILE -
C                     FOR24.DAT
C                 = 0  NO MODIFICATION
C                 = 1  MODIFY ONE GROUP OF ENERGIES
C               FOR MENGY = 1  OPERATOR RECEIVES PROMPT FOR:
C                 ME = FIRST ROW OF FOR24.DAT TO BE MODIFIED
C                 MF = LAST ROW OF FOR24.DAT TO BE MODIFIED
C                 SCALE3 - NUMBER TO MULTIPLY AUGER ENERGIES
C                          IN RANGE ME TO MF BY.
C
C         INTERNAL
C             ALL INTERNAL VARIABLES ARE DESCRIBED IN BODY
C             OF PROGRAM.
```

```
13900   C
14000   C
14100   C ***** COMMENT:  A SIMPLE WAY TO SEPARATE INDIVIDUAL CONTRIBU-
14200   C       TIONS OF TARGET SUBSHELLS IS TO INTRODUCE A LINE #12750
14300   C                          82    NORB = MIN
14400   C       AND TO REMOVE THE '82' FROM LINE #12800
14500   C
14600   C
14700   C ***** OUTPUT
14800   C       THE RESULTS OF THE CALCULATION, THE RTE CROSS SECTION
14900   C       SPECTRUM CONSISTING OF A TABLE OF CROSS SECTIONS AND
15000   C       THE ENERGIES TO WHICH THEY CORRESPOND, IS READ INTO
15100   C       FOR23.DAT.  THE CROSS-SECTIONS ARE GIVEN IN UNITS OF
15200   C       BARNS AND THE PROJECTILE ENERGIES ARE IN UNITS OF MEV.
15300   C
15400   C       IF A PLOT OF THE RESULTING SPECTRUM IS DESIRED, TYPE
15500   C       THE FOLLOWING:  ('.' = MONITOR PROMPT AND '--' = MINTAB
15600   C               PROMPT)
15700   C               .RUN PUB:MINTAB
15800   C               -- READ'FOR23.DAT'=C1,C2
15900   C               -- PLOT C1 VS C2
16000   C               -- STOP
16100   C       THE COMPUTER WILL DO THE REST
16200   C
16300   C
16400   C ***** REFERENCES
16500   C       1.  BRANDT, D.  PHYS REV A VOL 27, 3  P.1314 (1983)
16600   C
16700   C       2.  MCLAUGHLIN AND HAHN - TABLE FOR SI(+11) AND S(+13)
16800   C           AVAILABLE FROM J.A. TANIS
16900   C
17000   C       3.  F. BIGGS, ET. AL., AT. DATA NUCL. DATA TABLES 16,
17100   C           (1975)
17200   C
17300
17400
17500
17600
17700           DIMENSION DRER(21,2),QPIZ(31),EPR(200),SPECT(200,2)
17800           DIMENSION CPJ(31,17),Y(17)
17900   C
18000   C       ***** PROMPT INFORMATION FROM OPERATOR
18100           WRITE (5,510)
18200     510   FORMAT(/2X,'ENTER ATOMIC NO. OF PROJECTILE. FORMAT = I')
18300           READ(5,511) NOPROJ
18400     511   FORMAT (I)
18500           IF (NOPROJ.EQ.14) GO TO 88
18600           WRITE (5,72)
18700      72   FORMAT (/2X,'DO YOU WISH TO ALTER DR CROSS-SECTIONS FROM
18800        C THOSE OF S(+13)?'/2X,'NO = 0,  ALTER ONE GROUP = 1,  ALTE
18900        CR TWO GROUPS = 2')
19000           READ (5,531) MYES
19100           IF (MYES.EQ.0) GO TO 76
19200           WRITE (5,77)
19300      77   FORMAT (/2X,'ENTER RANGE OF TRANSITIONS TO BE CHANGED, A
19400        CND MULTIPLYER'/2X,'ONCE OR TWICE FOR ONE OR TWO GROUPS OF
19500        CTRANSITIONS'/2X,'AS FOLLOWS:   I,I,F'/2X,'MEANS MULTIPLY D
19600        CR CROSS-SECTIONS -I- THROUGH -I- BY F')
19700           IF (MYES.EQ.1) GO TO 74
19800           READ (5,75) MC,MD,SCALE2
19900      74   READ (5,75) MA,MB,SCALE1
20000      75   FORMAT (I,I,F)
20100      76   CONTINUE
20200      88   CONTINUE
20300           WRITE (5,91)
20400      91   FORMAT(/2X,'DO YOU WISH TO ALTER AUGER ENERGIES FOR ANY
20500        CTRANSITIONS '/2X,'IN PROJECTILE DATA FILE?'/2X,'NO = 0,
YES =
20600        C1')
```

```
20700           READ (5,444) MENGY
20800      444  FORMAT(I)
20900           IF (MENGY.EQ.0) GO TO 92
21000           WRITE (5,93)
21100       93  FORMAT (/2X,'ENTER RANGE OF TRANSITION ENERGIES TO BE CH
21200         CANGED, AND MULTIPLYER'/2X,'AS FOLLOWS: I,I,F'/2X,'MEANS MU
21300         CLTIPLY AUGER ENERGIES FOR TRANSITIONS -I- THROUGH -I- BY F
21400         C')
21500           READ (5,75) ME,MF,SCALE3
21600       92  CONTINUE
21700           WRITE (5,530)
21800      530  FORMAT(/2X,'ARE WE INCLUDING 1S, 2S, 2P ELECTRONS?,'/
21900          C  ' INCLUDE ALL =1   EXCLUDE: 1S=2, 1S,2S=3, 1S,2S,2P=5')
22000           READ (5,531) MIN
22100      531  FORMAT(I)
22200           WRITE (5,540)
22300      540  FORMAT(/2X,'WHICH TARGET? XE=17, AR=5, NE=3, HE=1, H=0')
22400           READ(5,531) NORB
22500           WRITE (5,720)
22600      720  FORMAT(/2X,'ENTER ENERGY RANGE IN MEV -MIN(I),MAX(I)')
22700           READ (5,542) MINEN,MAXEN
22800      542  FORMAT (I,I)
22900           WRITE(5,721)
23000      721  FORMAT(/2X,'ENTER STEP SIZE FOR ENERGY(MEV) - FORMAT I'/
23100          C  2X,'CONDITION IS:[(MAX - MIN)/STEP] MAY NOT EXCEED 200')
23200           READ (5,531) MEEV
23300    C
23400    C      SIGRTE = CROSS SECTION FOR RTE
23500    C      ELM = ELECTRON MASS IN ATOMIC UNITS
23600           SIGRTE=0.0E00
23700           ELM=1.0E+00
23800    C
23900    C      **** CALCULATE MASS OF PROJECTILE IN A.U.
24000    C      PRM = PROJECTILE MASS
24100           IF(NOPROJ.NE.23) GO TO 19
24200           PRM=50.90/(6.023E23*9.10E-28)
24300           GO TO 99
24400       19  IF(NOPROJ.NE.18) GO TO 29
24500           PRM=39.95/(6.023E23*9.10E-28)
24600           GO TO 99
24700       29  IF(NOPROJ.NE.22) GO TO 39
24800           PRM=47.90/(6.023E23*9.10E-28)
24900           GO TO 99
25000       39  IF(NOPROJ.NE.26) GO TO 49
25100           PRM=55.85/(6.023E23*9.10E-28)
25200           GO TO 99
25300       49  IF(NOPROJ.NE.21) GO TO 59
25400           PRM=44.96/(6.023E23*9.10E-28)
25500           GO TO 99
25600       59  PRM=(FLOAT(NOPROJ)*2.)/(6.023E23*9.108E-28)
25700
25800    C      DEPS = DELTA EPSILON FROM BRANDTS PAPER AND HAHNS
25900    C              NUMBERS - REQUIRED FOR PROJECTILE DATA CURRENTLY
26000    C              USED.
26100       99  DEPS=0.5E00
26200    C
26300    C      ***** WRITE INPUT TO OPERATOR FOR CONFIRMATION
26400           WRITE(5,550)
26500      550  FORMAT(///5X,'THIS IS WHAT WAS GIVEN ---------------')
26600           IF(NOPROJ.EQ.26) WRITE(5,451)
26700      451  FORMAT(2X,'THE PROJECTILE IS IRON(+23)')
26800           IF(NOPROJ.EQ.23)WRITE(5,452)
26900      452  FORMAT(2X,'THE PROJECTILE IS VANADIUM(+20)')
27000           IF(NOPROJ.EQ.22) WRITE(5,453)
27100      453  FORMAT(2X,'THE PROJECTILE IS TITANIUM(+19)')
27200           IF(NOPROJ.EQ.21)WRITE(5,454)
27300      454  FORMAT(2X,'THE PROJECTILE IS SCANDIUM(+18)')
27400           IF(NOPROJ.EQ.20) WRITE(5,455)
```

```
27500      455   FORMAT(2X,'THE PROJECTILE IS CALCIUM(+17)')
27600            IF(NOPROJ.EQ.18)WRITE(5,450)
27700      450   FORMAT(2X,'THE PROJECTILE IS ARGON(+15)')
27800            IF (NOPROJ.EQ.16) WRITE (5,551)
27900      551   FORMAT(2X,'THE  PROJECTILE IS SULFUR(+13)')
28000            IF(NOPROJ.EQ.14) WRITE(5,552)
28100      552   FORMAT (2X,'THE PROJECTILE IS SILICON(+11)')
28200            IF (NORB.EQ.17) WRITE(5,701)
28300      701   FORMAT(2X, 'THE TARGET IS XENON')
28400            IF(NORB.EQ.5) WRITE (5,556)
28500      556   FORMAT(2X,'THE TARGET IS ARGON')
28600            IF(NORB.EQ.3) WRITE(5,557)
28700      557   FORMAT(2X,'THE TARGET IS NEON')
28800            IF(NORB.EQ.1) WRITE(5,558)
28900      558   FORMAT(2X,'THE TARGET IS HELIUM')
29000            IF (NORB.EQ.0) WRITE (5,81)
29100       81   FORMAT(2X,'THE TARGET IS HYDROGEN')
29200            IF(MIN.EQ.1) WRITE (5,554)
29300      554   FORMAT(2X,'WE ARE INCLUDING ALL OF THE ELECTRONS')
29400            IF(MIN.EQ.2) WRITE(5,555)
29500      555   FORMAT(2X,'WE ARE NOT INCLUDING THE 1S ELECTRONS')
29600            IF(MIN.EQ.3) WRITE(5,702)
29700      702   FORMAT(2X,'WE ARE NOT INCLUDING THE 1S OR 2S ELECTRONS')
29800            IF(MIN.EQ.5) WRITE(5,703)
29900      703   FORMAT(2X,'WE ARE NOT INCLUDING 1S,2S, OR 2P ELECTRONS')
30000            WRITE (5,559) MINEN,MAXEN
30100      559   FORMAT(2X,'PROJ. ENERGY RANGE: ',I3,' TO ',I3,' MEV')
30200            WRITE(5,560) MEEV
30300      560   FORMAT (2X,'THE STEP SIZE BETWEEN ENERGY POINTS IS ',I2)
30400            WRITE(5,353)
30500      353   FORMAT(2X,'TYPE -- .TY FOR23.DAT -- FOR RESULT')
30600    C
30700    C       ***** READ DATA FILES
30800    C       **** READ COMPTON PROFILE
30900    C       ** XENON TARGET
31000            IF (NORB.NE.17) GO TO 12
31100            OPEN(UNIT=28,DEVICE='DSK',ACCESS='SEQIN',MODE='ASCII')
31200            IF (NORB.NE.17) GO TO 12
31300            DO 13 I=1,31
31400            READ (28,15) CPJ(I,1), CPJ(I,2),CPJ(I,3),CPJ(I,4),CPJ(I,
31500          C 5),CPJ(I,6),CPJ(I,7),CPJ(I,8),CPJ(I,9),CPJ(I,10),CPJ(I,1
31600          C 1),CPJ(I,12),CPJ(I,13),CPJ(I,14),CPJ(I,15),CPJ(I,16),CPJ
31700          C (I,17)
31800       15   FORMAT(6E10.3,/,6E10.3,/,5E10.3)
31900            IF(I.EQ.10.OR.I.EQ.20) WRITE(5,992) CPJ(I,10),CPJ(I,15)
32000      992   FORMAT (2E10.3)
32100       13   CONTINUE
32200            CLOSE (UNIT=28,DEVICE='DSK')
32300            GO TO 26
32400    C       ** ARGON TARGET
32500       12   IF (NORB.NE.5) GO TO 21
32600            DO 20 I=1,31
32700            READ(20,10)CPJ(I,1),CPJ(I,2),CPJ(I,3),CPJ(I,4),CPJ(I,5)
32800       10   FORMAT(5E10.3)
32900       20   CONTINUE
33000            GO TO 26
33100    C       ** NEON TARGET
33200       21   IF(NORB.NE.3) GO TO 27
33300            DO 23 I=1,31
33400            READ(21,22) CPJ(I,1),CPJ(I,2),CPJ(I,3)
33500       22   FORMAT(3E10.3)
33600       23   CONTINUE
33700            GO TO 26
33800       27   IF (NORB.NE.1) GO TO 69
33900    C       ** HELIUM TARGET
34000            DO 25 I=1,31
34100            READ (22,24) CPJ(I,1)
34200       24   FORMAT(E10.3)
34300       25   CONTINUE
34400            GO TO 26
```

```
34500   C       ** HYDROGEN TARGET
34600      69   OPEN(UNIT=26,DEVICE='DSK',ACCESS='SEQIN',MODE='ASCII')
34700           DO 28 I=1,31
34800           READ(26,30) CPJ(I,1)
34900      30   FORMAT(E10.3)
35000      28   CONTINUE
35100           CLOSE(UNIT=26,DEVICE='DSK')
35200      26   CONTINUE
35300   C
35400   C       ***** READ PROJECTILE INFORMATION FILE
35500   C       **** READ AUGER ENERGY, DR CROSS SECTION - SCALE IF
35600   C            DESIRED - PRINT TABLE OF FINAL DATA USED.
35700           WRITE (5,71) NOPROJ
35800      71   FORMAT(/5X,'DATA USED FOR PROJECTILE Z = ', I2//'     AU
35900        CGER ENERGY - DR CROSS-SECTIONS')
36000      41   DO 42 I=1,21
36100           READ(24,43) DRER(I,1),DRER(I,2)
36200           IF (NOPROJ.EQ.14) GO TO 67
36300           DRER(I,1) = (DRER(I,1))*((FLOAT(NOPROJ)/16.)**2)
36400           IF (MYES.EQ.0) GO TO 67
36500           IF (MYES.EQ.1) GO TO 78
36600           IF (I.LT.MC.OR.I.GT.MD) GO TO 78
36700           DRER(I,2) = DRER(I,2)*SCALE2
36800      78   IF (I.LT.MA.OR.I.GT.MB) GO TO 67
36900           DRER(I,2) = DRER(I,2)*SCALE1
37000      67   CONTINUE
37100           IF (MENGY.EQ.0) GO TO 94
37200           IF (I.LT.ME.OR.I.GT.MF) GO TO 94
37300           DRER(I,1) = DRER(I,1)*SCALE3
37400      94   CONTINUE
37500           WRITE (5,43) DRER(I,1),DRER(I,2)
37600           DRER(I,1)=DRER(I,1)/2.72E01
37700      43   FORMAT(2E16.4)
37800      42   CONTINUE
37900      44   CONTINUE
38000   C
38100   C       **** READ MOMENTUM VALUE FROM COMPTON PROFILE TABLE
38200           OPEN(UNIT=25,DEVICE='DSK',ACCESS='SEQIN',MODE='ASCII')
38300           DO 60 I=1,31
38400           READ(25,50) QPIZ(I)
38500      50   FORMAT(F6.2)
38600      60   CONTINUE
38700           CLOSE(UNIT=25,DEVICE='DSK')
38800   C       ****CLEAR EPR AND SPECT
38900   C
39000   C
39100   C       ********  CALCULATION STARTS ABOUT HERE
39200           EPR(1)=0.0E00
39300           DO 70 I=1,200
39400           SPECT(I,1)=0.0E00
39500           SPECT(I,2)=0.0E00
39600      70   CONTINUE
39700
39800   C       *** CALCULATE PROJECTILE ENERGY AND READ INTO EPR
39900   C       MCOUNT = NUMBER OF ENERGY POINTS WILL BE CALCULATED
40000           MCOUNT=(MAXEN-MINEN)/MEEV
40100           EEV=FLOAT(MEEV)*1.0E06
40200           DO 80 I=1,MCOUNT
40300           EPR(I) = ((EEV*FLOAT(I))+(FLOAT(MINEN)*1.0E06))/2.72E01
40400      52   FORMAT (E16.4)
40500      80   CONTINUE
40600
40700   C       **** COMPUTE CURVE FOR ONE PAIR OF DR CROSS SECTION,
40800   C            AUGER ENERGY
40900           DO 400 J=1,21
41000   C       **** SWEEP PROJECTILE ENERGY VALUES FROM MINEN TO MAXEN
41100           DO 500 I=1,MCOUNT
```

```
41200   C       PIZ = RELATIVE MOMENTUM ALONG BEAM AXIS
41300           PIZ=(DRER(J,1)-(EPR(I)*ELM)/PRM)*SQRT(PRM/(2.*EPR(I)))
41400           PIZ=ABS(PIZ)
41500   C       **** COMPARE PIZ TO QPIZ - INTERPOLATE TO FIND J(Q)
41600   C            VALUE CORRESPONDING TO PIZ.
41700           L=1
41800           NHY=1
41900     101   IF(QPIZ(L).LE.PIZ) GO TO 100
42000   C       SUMJQ=SUM OF COMPTON PROFILE FOR CONTRIBUTING ELECTRONS
42100           SUMJQ=0.0E00
42200           LL=L-1
42300           X1=QPIZ(LL)
42400           X2=QPIZ(L)
42500           IF (NORB.GT.0) GO TO 82
42600           NHY=NORB
42700           NORB=NORB+1
42800      82   DO 105 K=MIN,NORB
42900           Y(K)=0.0E00
43000           Y1=CPJ(LL,K)
43100           Y2=CPJ(L,K)
43200   C       **** POINT-SLOPE FORMULA
43300           Y(K)=((Y2-Y1)/(X2-X1))*(PIZ-X1)+Y1
43400   C       **** SUM ACCORDINGLY AS TO WHETHER ELECTRON IS IN S OR P
43500   C            STATE (K=1,2,4 FOR S, K=3,5 FOR P)
43600           IF (NORB.EQ.17) GO TO 218
43700           GO TO(102,102,103,102,103),K
43800     102   Y(K)=Y(K)*2.
43900           IF(NHY.NE.0) GO TO 104
44000           Y(K)=Y(K)/2.
44100           GO TO 104
44200     103   Y(K)=Y(K)*6.
44300           GO TO 104
44400     218   GO TO (1,1,1,2,1,1,2,2,3,1,1,2,2,3,1,1,2),K
44500       1   Y(K)=Y(K)*2.
44600           GO TO 104
44700       2   Y(K)=Y(K)*4.
44800           GO TO 104
44900       3   Y(K)=Y(K)*6.
45000     104   SUMJQ=SUMJQ+Y(K)
45100     105   CONTINUE
45200           GO TO 200
45300     100   L=L+1
45400           LMAX=31
45500           IF(L.NE.LMAX) GO TO 101
45600   C       **** IF PIZ IS GREATER THAN THE MAXIMUM VALUE OF QPIZ,
45700   C            SET SUMJQ=0
45800           SUMJQ=0.0E00
45900   C
46000   C       **** CALCULATE RTE CROSS SECTION
46100     200   SIGRTE=SQRT(PRM/(2.*EPR(I)))*DEPS*DRER(J,2)*SUMJQ
46200   C
46300   C       **** ENTER RTE CROSS SECTION AND EPR PAIRS INTO SPECT
46400   C            ARRAY.  OVERLAY EACH RTE CS VALUE FOR COMPLETE
46500   C            CURVE.
46600           SPECT(I,1)=SIGRTE+SPECT(I,1)
46700           SPECT(I,2)=(EPR(I)*2.72E+01)/1.0E06
46800     500   CONTINUE
46900   C       **** DO 500 LOOP FINISHED MEANS WE HAVE CALCULATED ALL
47000   C            ENERGY POINTS FOR ONE PAIR OF DATA, I.E.  ONE
47100   C            RESONANCE STATE.
47200     400   CONTINUE
47300   C       **** DO 400 LOOP FINISHED MEANS WE HAVE ENTIRE RTE
47400   C            CROSS SECTION CURVE.
47500   C       **** READ SPECT INTO DATA FILE FOR23.DAT
47600           DO 150 I=1,MCOUNT
47700           WRITE(23,1001) SPECT(I,1),SPECT(I,2)
47800    1001   FORMAT(F14.4,F10.2)
47900     150   CONTINUE
48000           STOP
48100           END
```

APPENDIX B

SAMPLE EXPERIMENTAL CALCULATIONS

The calculation of all plotted cross sections and ratios for S(13+) + He at 110 MeV which appear in this thesis is illustrated.

The linear plots of fraction i vs. pressure (Fig. 17) have slopes, m_i, errors, Δ_i, and percent errors, $\Delta_i(\%)$, as follows:

i	m_i	Δ_i	$\Delta_i(\%)$
$K\alpha$	3.57×10^{-8}	1.97×10^{-10}	3.0
$K_{\alpha+\beta}$	4.33×10^{-8}	7.71×10^{-11}	2.0
q,q-1	5.55×10^{-6}	3.66×10^{-9}	6.6
q,q+1	2.29×10^{-5}	8.47×10^{-7}	5.0
$(q,q-1)^{coinc.}_{K_{\alpha+\beta}}$	3.04×10^{-9}	7.98×10^{-11}	5.0
$(q,q+1)^{coinc.}_{K_{\alpha+\beta}}$	1.89×10^{-9}	1.12×10^{-10}	5.9
$(q,q-1)^{coinc.}_{K_{\alpha}}$	2.93×10^{-9}	6.14×10^{-11}	5.0
$(q,q+1)^{coinc.}_{K_{\alpha}}$	1.71×10^{-9}	6.13×10^{-11}	5.0

Errors represent uncertainties in the slopes resulting from a linear least squares fit (least squares program written by W.G. Graham). All slopes of fractions involving x rays have been multiplied by an experimentally determined dead time correction factor of 1.01.

The slopes and uncertainties in the slope are then multiplied by the constant, C_i (see eqns. 4.4, 4.5, and 4.6), to yield the cross sections, σ_i. In the calculation of C_i, the constant N is equal to 3.3×10^{13} atoms/cm$^2\mu$, ℓ is 1.83 cm for capture and loss cross sections

and 1.27 cm for cross sections involving x rays. The value of ℓ for the x-ray cross sections is the geometric gas cell length while the larger value of ℓ (obtained from W.G. Graham in a private communication) for the capture and loss cross sections includes the effect of the entrance and exit aperture sizes on the effective gas cell length. For those cross sections involving the detection of x rays, $\Delta\Omega/4\pi$ is calculated to be 0.321 ($\Delta\Omega$ obtained from M. Clark, private communication). The SiLi detector efficiency, ε, was interpolated by E. Bernstein from the data of Veigele to be 0.544 for K_α x rays and 0.663 for $K_{\alpha+\beta}$ x rays. Calculated values of C_i and the resulting cross sections follow:

i	C_i	σ_i
$K\alpha$	5.36×10^{-13}	1.93×10^{-20}
$K_{\alpha+\beta}$	5.26×10^{-13}	2.30×10^{-20}
q,q-1	1.66×10^{-14}	9.22×10^{-20}
q,q+1	1.66×10^{-14}	3.80×10^{-19}
$(q,q-1)^{coinc.}_{K\alpha+\beta}$	5.26×10^{-13}	1.62×10^{-21}
$(q,q+1)^{coinc.}_{K\alpha+\beta}$	5.26×10^{-13}	1.00×10^{-21}
$(q,q-1)^{coinc.}_{K\alpha}$	5.36×10^{-13}	1.59×10^{-21}
$(q,q+1)^{coinc.}_{K\alpha}$	5.36×10^{-13}	9.26×10^{-22}

For cross sections with large counting statistics, the counting error is generally found to be negligible when compared to the error in the slopes. However, the calculated error in the slopes for some of the fractions at 110 MeV is very low. The following errors were imposed as the minimum percent errors, taking into consideration counting statistics, slight fluctuations in $K_\alpha/K_{\alpha+\beta}$, dead time, averaging

of two sets of capture and loss data, and other relative experimental uncertainties: 3% for K_{α}, 2% for $K_{\alpha+\beta}$, 5% for q,q±1, and 5% for $(q,q\pm1)^{coinc.}_{K_{\alpha},\ K_{\alpha+\beta}}$. The errors shown in Figure 20b represent the statistical uncertainty of the total particle counts.

BIBLIOGRAPHY

Belic, D.S., Dunn, G.H., Morgan, R.J., Mueller, D.W., and Timmer, C. (1983). Dielectronic recombination: A crossed-beams observation and measurement of cross section. Physical Review Letters, 50, 339-342.

Bernstein, E.M., Oglesby, C.S., Tanis, J.A., Graham, W.G., Clark, M., McFarland, R.H., Morgan, T.J., Johnson, B.M., Jones, K.W. and Meron, M. (1984). Resonant electron transfer and excitation for S(13+) + He collisions. Bulletin of the American Physical Society, 29, 776.

Biggs, F., Mendelsohn, L.B., and Mann, J.B. (1975). Hartree-Fock Compton profiles for the elements. Atomic Data and Nuclear Data Tables, 16, 201-309.

Bitter, M., Hill. K.W., Sauthoff, N.R., Efthimion, P.C., Meservey, E., Roney, W., von Goeler, S., Horton, R., Goldman, M. and Stodiek, W. (1979). Dielectronic satellite spectrum of heliumlike iron (FeXXV). Physical Review Letters, 43, 129-132.

Brandt, D. (1983a). Resonant transfer and excitation in ion-atom collisions. Physical Review A, 27, 1314-1318.

Brandt, D. (1983b). A simple classical model for the impact parameter dependence of electron capture. Nuclear Instruments and Methods, 214, 93-96.

Burgess, A. (1964). Dielectronic recombination and the temperature of the solar corona. Astrophysical Journal, 139, 776-779.

Burgess, A. (1965). A general formula for the estimation of dielectronic recombination coefficients in low-density plasmas. Astrophysical Journal, 141, 1588-1590.

Clark, M., Brandt, D., Shafroth, S.M. (1984). Resonant and nonresonant transfer and excitation (RTE and NTE) in Si(11+) on He, Ne, Ar. Bulletin of the American Physical Society, 29, 777.

Dittner, P.F., Datz, S., Miller, P.D., Moak, C.D., Stelson, P.H., Bottcher, C., Dress, W.B., Alton, G.D., and Neskovic, N. (1983). Cross sections for dielectronic recombination of B(2+) and C(3+) via $2s \rightarrow 2p$ excitation. Physical Review Letters, 51, 31-34.

Feagin, J.M., Briggs, J.S., and Reeves, T.M. (1984). Simultaneous charge transfer and excitation. Journal of Physics B, 17, 1057-1068.

Hasted, J.B. (1972). Physics of atomic collisions (2nd ed.). New York: Elsevier.

LaGattuta, K. and Hahn, Y. (1983). Dielectronic recombination rates for Ar(14+). Physical Review A, 27, 1675-1677.

McLaughlin, D.J., and Hahn, Y. (1982). Dielectronic recombination cross sections for Si(11+) and S(13+). Physics Letters, 88A, 394-397.

Merts, A.L., Cowan, R.D., and Magee, N.H. Jr. (1976). The calculated power output from a thin iron-seeded plasma. Unpublished, Los Alamos Scientific Laboratory Informal Report LA-62200-MS.

Merzbacher, E. (1970). Quantum mechanics (2nd ed.). New York: John Wiley & Sons.

Mitchell, J.B.A., Ng, C.T., Forand, J.L., Levac, D.P., Mitchell, R.E., Sen, A., Miko, D.B., and McGowan, J. Wm. (1983). Dielectronic recombination cross-section measurements for C+ ions. Physical Review Letters, 50, 335-338.

Nasser, I., and Hahn, Y. (1983). Dielectronic recombination rates for heliumlike ions. Journal of Quantum Spectroscopy and Radiation Transfer, 29, 1-8.

Oglesby, C. Sloan, Bernstein, E.M., and Tanis, J.A. (1984). Calculated resonant-transfer-and-excitation cross sections for lithiumlike projectiles incident on helium. Bulletin of the American Physical Society, 29, 743.

Pepmiller, P.L. (1983). Formation of doubly excited two electron ions during F(8+) + He, Ne, or Ar collisions. Doctoral dissertation, Kansas State University, Manhattan, KS.

Post, D.E. (1981). Physics of ion-ion and electron-ion collisions. New York: Plenum Press.

Roszman, L.J. (1979). Dielectronic recombination rate of Mo XXXIII. Physical Review A, 20, 673-676.

Seaton, M.J., and Storey, P.J. (1976). Dielectronic recombination. In P.G. Burke and B.L. Moiseiwitsch (Eds.), Atomic processes and applications (pp. 133-197). New York: North Holland Publishing.

Sellin, I.A. (Ed.). (1979). Structure and collisions of ions and atoms. New York: Springer-Verlag.

Tanis, J.A., Bernstein, E.M., Graham, W.G., Clark, M., Shafroth, S.M., Johnson, B.M., Jones, K.W., and Meron, M. (1982). Resonant behavior in the projectile x-ray yield associated with electron capture in S + Ar collisions. Physical Review Letters, 49, 1325-1328.

Tanis, J.A., Bernstein, E.M., Graham, W.G., Stockli, M.P., Clark, M., McFarland, R.H., Morgan, T.J., Berkner, K.H., Schlacter, A.S., and Stearns, J.W. (1984). Resonant electron transfer and excitation in 2-, 3-, and 4-electron $_{20}Ca^{q+}$ and $_{23}V^{q+}$ ions colliding with helium. Physical Review Letters, 53, 2551-2554.

Tanis, J.A., Bernstein, E.M., Oglesby, C.S., Graham, W.G., Clark, M., McFarland, R.H., Morgan, T.J., Stockli, M.P., Berkner, K.H., Schlacter, A.S., Stearns, J.W., Johnson, B.M., Jones, K.W., and Meron, M. (in press). Resonant-transfer-and-excitation for highly charged ions ($16 \leq Z \leq 23$) in collisions with helium. Nuclear Instruments and Methods.

Tanis, J.A., Shafroth, S.M., Willis, J.E., Clark, M., Swenson, J., Strait, E.M., and Mowat, J.R. (1981). Simultaneous electron capture and excitation in S + Ar Collisions. Physical Review Letters, 47, 828-831.

Veigele, Wm. J. (1973). Photon cross sections from 0.1 KeV to 1 MeV for elements Z=1 to Z=94. Atomic Data Tables, 5, 51-111.